HHS Public Access

Author manuscript

Cell Rep. Author manuscript; available in PMC 2020 December 10.

Published in final edited form as:

Cell Rep. 2020 October 27; 33(4): 108320. doi:10.1016/j.celrep.2020.108320.

In Vitro Recapitulation of Murine Thymopoiesis from Single Hematopoietic Stem Cells

Amélie Montel-Hagen[1,9], **Victoria Sun**[1,2,9], **David Casero**[1,8], **Steven Tsai**[3], **Alexandre Zampieri**[1], **Nicholas Jackson**[1], **Suwen Li**[1,4,5], **Shawn Lopez**[1], **Yuhua Zhu**[1], **Brent Chick**[1], **Chongbin He**[1], **Stéphanie C. de Barros**[1], **Christopher S. Seet**[3,5,6], **Gay M. Crooks**[1,5,6,7,10,*]

[1]Department of Pathology & Laboratory Medicine, David Geffen School of Medicine, University of California, Los Angeles (UCLA), Los Angeles, CA, USA

[2]Molecular Biology Interdepartmental Program, UCLA, Los Angeles, CA, USA

[3]Division of Hematology-Oncology, Department of Medicine, David Geffen School of Medicine, UCLA, Los Angeles, CA, USA

[4]Department of Molecular and Medical Pharmacology, UCLA, Los Angeles, CA, USA

[5]Eli and Edythe Broad Center of Regenerative Medicine and Stem Cell Research, UCLA, Los Angeles, CA, USA

[6]Jonsson Comprehensive Cancer Center, UCLA, Los Angeles, CA, USA

[7]Division of Pediatric Hematology-Oncology, Department of Pediatrics, David Geffen School of Medicine, UCLA, Los Angeles, CA, USA

[8]Present address: F. Widjaja Foundation Inflammatory Bowel and Immunobiology Research Institute, Cedars-Sinai Medical Center, Los Angeles, CA, USA

[9]These authors contributed equally

[10]Lead Contact

SUMMARY

We report a serum-free, 3D murine artificial thymic organoid (M-ATO) system that mimics normal murine thymopoiesis with the production of all T cell stages, from early thymic progenitors to functional single-positive (CD8SP and CD4SP) TCRαβ and TCRγδ cells. RNA sequencing aligns M-ATO-derived populations with phenotypically identical primary thymocytes. M-ATOs initiated with *Rag1*$^{-/-}$ marrow produce the same differentiation block as seen in the endogenous thymus,

*Correspondence: gcrooks@mednet.ucla.edu.

AUTHOR CONTRIBUTIONS

Conceptualization, A.M.-H., V.S., C.S.S., and G.M.C.; Methodology, A.M.-H. and V.S.; Formal Analysis, D.C.; Investigation, A.M.-H., V.S., S.T., A.Z., N.J., S. Li, S. Lopez, Y.Z., B.C., and C.H.; Data Curation, D.C.; Writing – Original Draft, A.M.-H., V.S., and G.M.C.; Writing – Review & Editing, A.M.-H., V.S., C.S.S., S.C.D., and G.M.C.; Supervision, G.M.C.; Funding Acquisition, G.M.C.

SUPPLEMENTAL INFORMATION

Supplemental Information can be found online at https://doi.org/10.1016/j.celrep.2020.108320.

DECLARATION OF INTERESTS

A.M.-H., C.S.S., and G.M.C. are listed on patents relating to this work. A.M.-H., C.S.S., and G.M.C. are co-founders of PLUTO Immunotherapeutics.

and Notch signaling patterns in M-ATOs mirror primary thymopoiesis. M-ATOs initiated with defined hematopoietic stem cells (HSCs) and lymphoid progenitors from marrow and thymus generate each of the downstream differentiation stages, allowing the kinetics of T cell differentiation to be tracked. Remarkably, single HSCs deposited into each M-ATO generate the complete trajectory of T cell differentiation, producing diverse TCR repertoires across clones that largely match endogenous thymus. M-ATOs represent a highly reproducible and efficient experimental platform for the interrogation of clonal thymopoiesis from HSCs.

In Brief

Montel-Hagen et al. develop a murine artificial thymic organoid (M-ATO) system to reproduce thymopoiesis *in vitro* from bone marrow stem and progenitor cells (HSPCs). This method efficiently recapitulates the phenotypic and transcriptional features of normal murine T cell development even when initiated with a single HSC.

Graphical Abstract

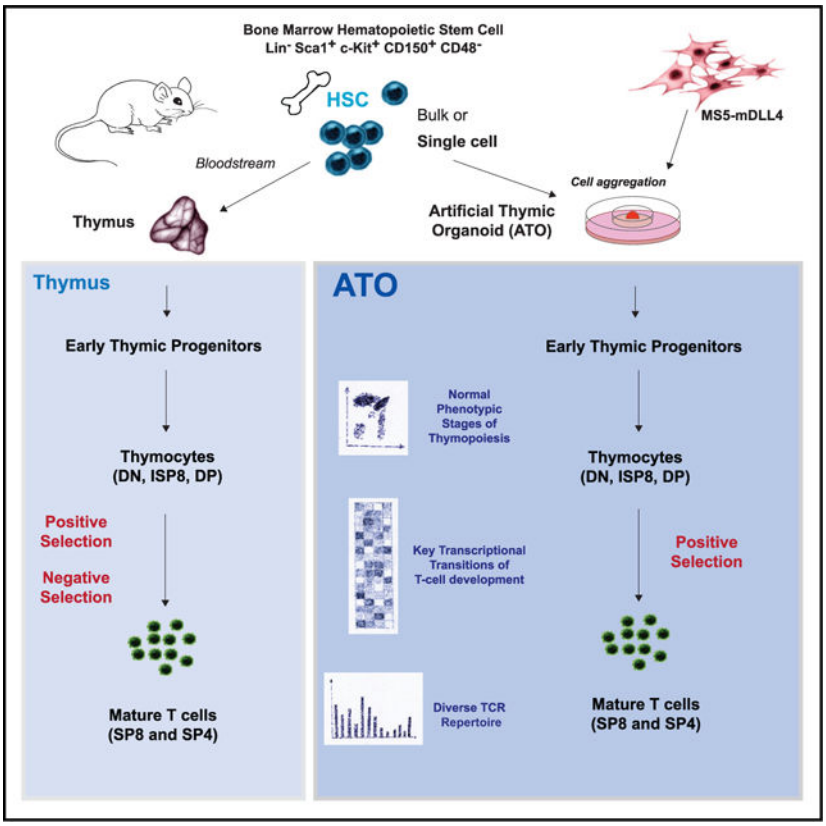

INTRODUCTION

Commitment to the T cell lineage begins in the thymus from stem and progenitor cells that have trafficked from the bone marrow and is induced by complex spaciotemporal interactions between precursor T cells and thymic epithelial cells, thymic mesenchyme, and other hematopoietic cells (Breed et al., 2018; Rothenberg et al., 2008; Takahama, 2006).

Among these interactions, Notch signaling from ligands in the thymic stroma (specifically Delta-like ligand 4 [DLL4]) is critical for the exclusive commitment of the progenitor cells to the T cell lineage (Hozumi et al., 2008; Koch et al., 2008; Taghon et al., 2006).

Several *in vitro* systems have been developed to try to mimic the thymic microenvironment's ability to induce and maintain T cell commitment and differentiation (Fan et al., 2015; Hare et al., 1999; Schmitt and Zúñiga-Pflücker, 2002). Among them, the OP9-DL1 monolayer co-culture system revolutionized the field, allowing the commitment of hematopoietic stem and progenitor cells (HSPCs) to the T cell lineage in a dish (Schmitt and Zúñiga-Pflücker, 2002). However, monolayer systems have shown limitations: positive selection and thus production of mature TCR$\alpha\beta^+$ cells, especially $CD4^+$ T cells, is very limited. In addition, reproducibility is affected by variations in serum-containing medium.

We have recently developed an artificial thymic organoid (ATO) model of *in vitro* T cell differentiation from human HSPCs (Seet et al., 2017) as well as human pluripotent stem cells (Montel-Hagen et al., 2019). Human ATOs reproducibly generate mature CD8 and CD4 T cells *in vitro* using three-dimensional (3D) aggregates of HSPCs with a standardized Notch ligand-expressing stromal cell line in serum-free conditions. However, results using identical conditions with murine cells are suboptimal. We now report a modified ATO system that allows the highly efficient differentiation of murine bone marrow HSPCs to mature T cells *in vitro*. Murine ATOs (M-ATOs) mimicked normal murine thymopoiesis with the production of all immature and mature T cell subsets, including TCR$\gamma\delta^+$ cells and conventional TCRβ^+ T cells (both CD8SP and CD4SP) and $FoxP3^+$ cells. Mature cells expressed CD62L, responded to TCR activation, and exhibited a broad TCR Vβ repertoire consistent with positive selection. RNA sequencing of the different M-ATO-derived T cell subsets revealed a transcriptional profile highly similar to that of primary T cell populations from the murine thymus. M-ATOs could recapitulate thymopoiesis from different subsets of BM and thymus progenitor populations. The high efficiency of the M-ATO system allowed the production of millions of T cells with a diverse repertoire from single highly purified HSCs.

Thus, M-ATOs are a technically simple, highly reproducible, and comprehensive platform to study the full range of murine T cell development and maturation from single HSPCs.

RESULTS

M-ATOs Recapitulate the Early Stages of Murine T Cell Development

To generate a robust and highly reproducible *in vitro* system that supports the earliest stages of murine T cell commitment as well as positive selection, we modified our previously developed serum-free ATO model (Montel-Hagen et al., 2019; Seet et al., 2017). MS5 stromal cells transduced with murine DLL4 (hereafter referred to as MS5-mDLL4) were aggregated with murine HSPCs (defined as Lin^- $Sca1^+$ $cKit^+$; hereafter referred to as LSK) from fresh or frozen C57BL/6 murine young adult (1–4 months) bone marrow and deployed on a cell culture insert at the air-liquid interface (Figure 1A).

In contrast to human ATOs, we identified DMEM-F12 as the optimal basal medium for murine cultures (Figure S1A). As in the human system, we used the B27 supplement as a replacement for fetal calf serum. This serum-free medium (hereafter referred to as D/F12-B27) was supplemented for the entire culture period, with Fms-related tyrosine kinase 3 (Flt3L), interleukin (IL)-7, ascorbic acid and beta mercapto-ethanol (BME) (Figure 1A); for the first week of culture, Stem Cell Factor (SCF) was also added.

M-ATOs induced commitment of HSPCs to the T cell lineage by week 2, while cells expressing markers of non-T cell lineages (CD11b, CD11c, GR1, CD19, B220, and NK1.1; hereafter referred to as Lin) decreased markedly (Figure 1B). M-ATOs rapidly produced γδ T cells, which later decreased in frequency as conventional TCRβ T cells were generated. The immature single-positive $CD8^+$ (ISP8) and $CD8^+CD4^+$ double-positive (DP) populations emerged from the $CD8^-$ $CD4^-$ double-negative (DN) cells between week 2 and week 3 and were maintained long term (Figures 1B and 1C).

Typically, cell numbers generated in M-ATOs peaked at week 3 with an average 12,000-fold increase when initiated with 500 LSK cells in a single ATO. Cell numbers slightly dropped at week 5 but remained constant until the end of the culture at week 8 (Figure 1C). Interestingly, a lower concentration (2%) of B27 supplement compared with that used in the human system (4%) was beneficial for longer term cultures (Figure S1B).

We analyzed subsets of the $CD4^-$ $CD8^-$ DN population over time using the standard CD44 and CD25 markers (Godfrey et al., 1993) (Figures 1B, 1D, and 1E). Daily analysis during the first 2 weeks of culture demonstrated progression of the cultures from the DN1 through DN4 stages, with DN3 cells predominating after the first week of culture (Figures 1D and 1E). A detailed analysis of the earliest stages using c-kit expression, as described by the Rothenberg group (Yui et al., 2010), further delineated progression through early thymic progenitors (ETPs), DN2a, and DN2b populations (Figure 1E; Figure S1C). DN3a and DN3b subsets could also be discriminated on the basis of either CD28 expression (Teague et al., 2010) or intracellular TCRβ (iTCRβ) (Taghon et al., 2006; Wilson et al., 1999) (Figure S1D).

T Cell Maturation in M-ATOs

Analysis of more mature T cells demonstrated the emergence of $CD3^+TCR\beta^+$ cells between week 2 and week 3 of culture. This population was maintained throughout culture and contained $CD4^+CD8^+$ (DP), $CD4^-$ $CD8^+$ (CD8SP), and $CD8^-$ $CD4^+$ (CD4SP) mature T cells (Figures 2A and 2B). A population of $CD3^+CD4^-CD8^-$ cells consistent with previously described innate T cells (Brandt and Hedrich, 2018; Yamamoto et al., 2019) was also observed (Figure 2A).

Forty percent to 80% of CD8SP T cells and 5%–15% of CD4SP T cells displayed a $CD62L^+$ $CD44^{lo}$ phenotype consistent with conventional mature naive T cell phenotype produced in the normal thymus (Bradley et al., 1994; Budd et al., 1987; Ley and Tedder, 1995) (Figure 2C). CD8SP and CD4SP $CD62L^+$ cells exhibited polyfunctional production of interferon (IFN)-γ, tumor necrosis factor alpha (TNF-α), and IL-2 in response to phorbol 12-myristate13-acetate (PMA) and ionomycin (Figure 2D). Both CD8SP and CD4SP

proliferated and upregulated the activation marker CD25 in response to anti-CD3/CD28 and IL-2 stimulation (Figure 2E).

Immunofluorescence staining of whole-mounted M-ATOs at week 4 demonstrated abundant $CD4^+$ and $CD8^+$ T-lineage cells interspersed with MS5-mDLL4 stromal cells (Figure 2F). Further analysis demonstrated the presence of DP, CD8SP, and CD4SP cells (Figures S2A and S2B).

M-ATOs do not contain thymic epithelial cells, which are responsible for the selection of CD4SP in the thymus through major histocompatibility complex (MHC) class II expression. Consistent with this, CD4SP were produced at lower frequency compared with the thymus (Figure 2B). We hypothesized that the ability to generate any CD4SP in M-ATOs was made possible by positive selection mediated via MHC class II-expressing hematopoietic cells generated from the HSPCs that initiated the ATOs. Indeed, the analysis of non-T-lineage cells in 5 week M-ATOs revealed that a small percentage of cells belonged to the myeloid lineage and that some expressed MHC class II molecules. As in the human system, M-ATOs produced some dendritic cells, but no B cells were detected in M-ATOs after 5 weeks (Figure S2C).

FoxP3 (Forkhead box P3) is a transcription factor specifically expressed in $CD4^+CD25^+$ regulatory T cells (Tregs) and required for their development (Fontenot et al., 2005). Six weeks after initiating M-ATOs with LSK cells from FoxP3 reporter mice, a subset of the CD4SP cells co-expressed GFP (Foxp3) and CD25, suggesting the production in M-ATOs of cells with a Treg phenotype (Figure 2G). Of the two phenotypic Treg precursors that have been described, $CD25^{neg}$ $Foxp3^+$ (Marshall et al., 2014; Tai et al., 2013) were at very low frequency, whereas a robust population of $CD25^+$ FoxP3 (Lio and Hsieh, 2008) was detected (Figure 2G).

T Cell Differentiation and TCR Diversity in M-ATOs Using Different Murine Backgrounds

The studies described above were performed with bone marrow cells harvested from C57BL/6 mice. There are known intrinsic differences between murine strains in terms of blood cell and T cell development, including CD4SP/CD8SP predominance (Petkova et al., 2008). To verify that the M-ATO model was applicable to other murine models, we compared the use of LSK cells harvested from the bone marrow of the C3H/He (the strain from which the MS5 stromal line was derived) (Itoh et al., 1989), BALB/c, and FVB murine strains. In all backgrounds, M-ATOs efficiently supported T cell differentiation, although with slightly different kinetics (Figure 3A; Figures S3A–S3C). C3H/He and FVB strains generated more CD4SP cells than CD8SP, typical of normal thymopoiesis, whereas in M-ATOs from C57BL/6 and BALB/c, CD8SP predominated relative to CD4SP (Figure 3A; Figures S3A–S3C).

Analysis of TCR diversity via Vβ expression revealed that both the CD8SP and CD4SP cells generated in M-ATOs from the four different murine backgrounds exhibited a broad repertoire (Figure 3B; Figure S3D). Vβ5.1,5.2, Vβ11, and Vβ12 TCR-bearing T lymphocytes are known to be clonally eliminated, either completely or partially, through negative selection in the thymi of C3H/He and BALB/c mice, but not in C57BL/6 or FVB

mice (Abe et al., 1991; Bill et al., 1989, 1990; Gao et al., 1989; Hodes and Abe, 2001; Sugihara et al., 1990; Tomonari et al., 1993; Vacchio and Hodes, 1989; Woodland et al., 1990, 1991). As expected, Vβ5.1,5.2, Vβ11, and Vβ12 expression was almost undetectable in endogenous thymocytes from C3H/He and BALB/c mice. In contrast, M-ATO-derived cells from C3H/He and BALB/c mice showed significantly increased cells expressing these Vβ segments (Figures 3B and 3C). M-ATOs derived from control C57BL/6 or FVB strains in which Vβ5.1,5.2, Vβ11, and Vβ12 TCR segments are not negatively selected in the thymus showed similar expression of these segments in endogenous thymocytes and M-ATO-derived T cells (Figure 3C). These data are consistent with a lack of negative selection during M-ATO-induced T cell differentiation with the potential for survival of more self-reactive T cells in ATOs.

Transcriptional Analysis of T Cell Differentiation in M-ATOs

Principal-component analysis (PCA) using global genome-wide expression profiles for all populations from M-ATOs, thymus (THY hereafter), and the Immgen dataset (Mingueneau et al., 2013) revealed the major transcriptional events known to operate during T cell development and the relatedness between thymic and M-ATO-derived populations (Figure 4A). The first principal component (PC1; 43% of total variance) fully correlated with the developmental progression from ETPs to positively selected cells. Top PC1-ranked genes (Figure 4B, left) included both legacy hematopoietic progenitor genes (*Cd34*, *Bcl11a*, *Hhex*, *Mpo*, and *Spi1*, among others), which were repressed after the ETP/DN2 stages, and genes upregulated during T cell lineage commitment and maturation (*Ikzf3*, *Id3*, *Cd2*, *Cd4*, and *Cd8* genes, among others). The second principal component (PC2; 26% of total variance) was associated with genes with peak or repressed expression in the transition from DN3 to DP cells (Figure 4A). PC2 segregated immature (ETP) and mature (single-positive) populations from those involved in the transitions around TCR re-arrangements. Top PC2-ranked genes included *Ptcra*, which encodes the pre-T cell antigen receptor alpha, along with the recombinase genes *Rag1/2*, among others (Figure 4B, right).

We next performed unsupervised hierarchical model-based clustering of thymic and M-ATO-derived populations. Because of differences in baseline gene expression, we normalized and compared the pattern of gene expression within and between thymus and M-ATO-derived samples in several ways. To capture all the sources of variability contributing to the PCA map above, we first classified the genes by their overall expression profile, using an unsupervised approach and stringent thresholds. We then identified a set of most variable genes (2,554 mouse genes) using pairwise statistical tests within (e.g., THY-ETPs versus THY-DN2s), and between (THY-ETPs versus ATO-ETPs) each compartment. To better visualize gene expression trends, clusters were reordered to match peaked gene expression in the cluster with developmental stages (from ETPs to SPs) (Figure 4C). Hierarchical model-based clustering and heatmap visualization revealed that our approach captured a rich mosaic of expression profiles. As with the PCA, THY and M-ATO expression profiles were highly correlated overall and largely mimicked the profiles of reference populations from Immgen.

Model-based clustering was also performed on the combined dataset (THY+ATO) so that both compartments have the same weight on the obtained groups. We identified a total of 29 gene clusters (Table S1), with distinct expression profiles. The average normalized expression profile for all genes in select clusters are displayed, and representative genes in each cluster are listed (Figure 4D). Individual gene expression levels within each cluster are provided in Table S1. Our unsupervised classification recapitulated the expected behavior of genes with known functions in thymic T cell differentiation, both in THY and M-ATO-derived subsets.

Finally, gene set enrichment analyses (GSEAs) for selected transcriptional transitions revealed that the set of most regulated genes between developmentally proximal populations in THY and M-ATO samples were largely similar (Figure S4), both showing significant enrichment scores when compared against independent thymocyte gene signatures.

Rag1 Deficiency and Notch Signaling Patterns Are Recapitulated in M-ATOs

As the M-ATO system closely mirrors phenotypic and transcriptional T cell development in the primary thymus, we next assessed two signaling pathways that are critical for thymopoiesis.

First, we used a *Rag1* (recombination activating gene 1)-deficient ($Rag1^{-/-}$) mouse to test whether TCR-dependent developmental checkpoints still applied within the M-ATO system. In M-ATOs generated from $Rag1^{-/-}$ marrow LSK cells, DP cells were absent, matching the phenotype of the $Rag1^{-/-}$ thymus (Figures 5Ai and 5Aii) (Mombaerts et al., 1992). Both the M-ATO and thymus from $Rag1^{-/-}$ mice showed normal progression through the DN1/DN2 to the DN3 stage but a block in transition from DN3 to DN4 (Figures 5Bi and 5Bii). A small population of ISP8 cells (ISP8 cells: $CD3^{-}$ $CD4^{-}$ $CD8^{+}$) was also detected in both M-ATO and thymus from $Rag1^{-/-}$ mice. Although a DP population emerged later in culture (data not shown), CD3 and TCRβ were never expressed over the course of the culture, again consistent with $Rag1^{-/-}$ thymocytes (Figures 5Ci and 5Cii).

To determine whether Notch signaling during T cell development in the M-ATO resembles that of the endogenous thymus, we used LSK cells from a transgenic Notch reporter (TNR) mouse line (Nowotschin et al., 2013). In both endogenous thymocytes and M-ATO cells, Notch reporter activity fell from the DN2b to the DN3a stage and again during the DN3a to DN3b transition (Figures 5D and 5E); the latter marks the stage during which thymocytes undergo beta selection and when RNA expression of Notch targets is markedly decreased (Mingueneau et al., 2013; Taghon et al., 2006; Teague et al., 2010). Thus, the M-ATO system was able to recapitulate changes in Notch reporter activity in highly defined stages of T cell development.

The Kinetics of T Cell Differentiation Are Captured by Initiation of M-ATOs with Different Progenitor Populations

We next interrogated if the M-ATO system was able to recapitulate T cell development when seeded with different phenotypic progenitors in the hematopoietic hierarchy. From C57BL/6 bone marrow, the following phenotypes were tested in M-ATOs: HSC (LSK $IL7R^{-}$ $CD150^{+}$ $CD48^{-}$), MPPs (multi-potent progenitors) (LSK $IL7R^{-}$ CD150 $CD48^{-}$), LMPPs (lymphoid-

primed MPPs) (LSK IL7R^{+} Flk2^{+}), and CLPs (common lymphoid progenitors) (Lin^{-} c-Kit^{Lo} Sca^{Lo} IL7R^{+} Flk2^{+}). In addition, the following populations were isolated from thymus and tested in M-ATOs: ETPs (Lin^{-} c-Kit^{Hi} CD44^{Hi} CD25^{-}), DN2 (Lin^{-} CD4^{-} CD8^{-} c-Kit^{Hi} CD44^{Hi} CD25^{+}), and DN3 (Lin^{-} CD4^{-} CD8^{-} c-Kit^{-} CD44^{-} CD25^{+}). Analyses at weeks 1, 2, and 6 were performed to assess the kinetics of T cell development (Figures 6A–6D). At week 1, only M-ATOs initiated with the most T-committed population tested (thymic DN3) had reached the ISP8 and DP stages, while the M-ATO-derived cells initiated from all the other more immature subsets remained at the DN stage (Figures 6A and 6D). However, closer analysis of the DN subsets at week 1 showed that only HSC-initiated M-ATOs remained at the DN1 stage; MPP had generated a mix of DN1–3; LMPP, CLP and ETP had generated a mix of DN2 and DN3; only DN3 subsets remained in the M-ATOs initiated from DN2 and DN3 populations (Figure 6A; Figure S5A). By week 2 of culture, HSC and MPP-seeded M-ATOs were still almost entirely at the DN stage, whereas M-ATOs initiated from all the lymphoid progenitors (LMPP, CLP, and all thymic progenitors) had begun to produce DP cells and CD3^{+} TCRβ^{+} cells (Figures 6B and 6D). Within the DN cells that remained in cultures, a logical further progression through the subsequent stages was seen from each type of initiating cell (Figure S5B). By week 6, all hematopoietic subsets tested in M-ATOs had produced mature T cells (Figures 6C and 6D). A detailed time-course analysis of T cell differentiation from HSCs is shown in Figures S5C and S5D.

Interestingly, M-ATOs initiated with the most immature stem and progenitor cells (specifically HSCs, MPPs, and LMPPs) generated a higher frequency of CD4SP cells (Figure 6C; Figure S5E). CDSP4 output was barely detectable when initiating M-ATOs with CLPs and later populations.

The M-ATO System Supports Thymopoiesis from Isolated Single Cells

The efficiency of T cell differentiation in M-ATOs was next tested using limiting numbers of marrow LSK cells to initiate cultures with a fixed number of MS5-mDLL4 per M-ATO. The cell number and phenotype generated from each M-ATO was similar over a range of 4,000 to as few as 5 initiating LSK cells (Figure 7A). The observation that hematopoietic cells undergo a comparable amount of proliferation regardless of the initiating number of cells in the ATO was consistent throughout extensive studies. We therefore speculate that there are constraints related to the physical size of ATOs, possibly due to gas exchange and nutrient availability.

We next tested the feasibility of generating M-ATOs seeded with single fluorescence-activated cell sorting (FACS)-isolated LSK cells. Of 48 M-ATOs plated, 7 produced sufficient cells for analysis by week 3 (Figure 7B). All 7 of the M-ATOs analyzed revealed a phenotype consistent with T cell commitment (negative for other lineage markers and exhibiting the phenotype of DN populations). Clones showed variations in terms of cell number and stage of differentiation, reflecting the heterogeneity of the LSK HSC/progenitor population. As expected, greater cell numbers were observed in those clones that had already progressed to the DP stage at time of analysis (Figure 7B).

The ability of M-ATOs to support clonal T cell development from highly purified HSC was then tested by seeding single cells from the CD150^{+}CD48^{-} phenotypic subset of the LSK

population into each M-ATO. At week 3, the cloning efficiency was at least 12% (6 clones out of 48 M-ATOs could be analyzed) (Figure 7C); at this early time point, none of the M-ATOs had progressed past the DN stage (Figure 7C; Figure S6A). Interestingly however, the 3 week clones were not fully synchronized, with some still mostly at the DN1 stage and others already exclusively at the DN3 stage (Figure 7C; Figure S6A), suggesting that the cells within the HSC phenotype were at slightly different states of T lymphoid priming when isolated (Rothenberg, 2011). At weeks 6–7, depending on the technical efficiency of the single-cell seeding, 25%–49% of the M-ATOs showed cell growth, and all clones analyzed revealed T cell commitment, most of them containing DP and $TCR\beta^+CD3^+$ CD4SP and CD8SP (Figure 7D; Figures S6B–S6C). Cell output in single HSC-seeded M-ATOs ranged from 2×10^6 to 10×10^6 by weeks 6–7 (Figure 7D; Figure S6C). Intracellular detection of the Treg-associated transcription factor FOXP3 revealed that 4 of 6 analyzed M-ATOs seeded with a single HSC produced $CD4^+$ $CD25^+$ $Foxp3^+$ Treg-like cells (Figure 7E). Analysis of TCR diversity via Vβ expression by flow cytometry on 12 independent M-ATOs, each generated from a single HSC, revealed that both the CD8SP and CD4SP T cells produced in M-ATOs exhibited a broad repertoire, with a similar pattern of Vβ use seen across M-ATO clones (Figure 7F) and in bulk cultures and normal thymus of the same C57BL/6 strain (Figure 3B).

DISCUSSION

We have shown here a simple and powerful *in vitro* model of murine T cell differentiation that faithfully recapitulates the exquisitely controlled progression of key phenotypic and transcriptional events that define normal thymopoiesis. The quantitative and temporal consistency of the M-ATO system provides an experimental platform that can be used to test how extrinsic and intrinsic factors affect the process of T cell commitment and maturation. The M-ATO system allows the rigorous interrogation of T cell potential in highly purified HSC and progenitor populations, including LMPP and CLP from the marrow, and multipotent and T cell committed progenitors in the thymus. Impressively, M-ATOs seeded with single HSCs were able to generate a diverse array of mature thymocytes, including $TCR\beta^+$, polyclonal CD4SP and CD8SP, and $FOXP3^+$ $CD4^+CD25^+$ cells.

Despite the remarkable fidelity in the transcriptional profiling of populations from normal thymus and M-ATOs, a few subtle differences were noted. $TCR\beta^+CD3^+$ DP cells from M-ATOs partially overlapped transcriptionally with the more immature $TCR\beta^-CD3^-$ DP population from endogenous thymus, possibly because of earlier surface expression of TCRβ/CD3 on DP cells in the M-ATO. Also, basal expression of genes known to be transcriptional targets of Notch signaling was higher in M-ATO populations. Nonetheless, the overall transcriptional profile of Notch targets during T cell development was conserved, and the pattern of Notch signaling seen in the ATO using the TNR mouse model closerly mirrored that of *in vivo* thymus.

On the basis of an *in vivo* thymic implant model, cellular turnover for the replacement of thymocytes in the mouse thymus has been estimated to take 4 weeks (Berzins et al., 1998). The kinetics of T cell development were similar in the M-ATOs, with the generation from HSC of all stages of thymocytes including single-positive cells by week 4. The more

immature the initiating population, the slower the onset of T cell development, with at least 2 extra weeks in lag time seen with highly purified HSCs compared with the more lymphoid committed progenitors LMPP and CLP.

Unlike the endogenous thymus (Boehm, 2012; Love and Bhandoola, 2011; Rothenberg, 2019), the M-ATOs are not constantly seeded with bone marrow progenitors; however, T cell production can be maintained in M-ATOs for several weeks. Thymus transplantation experiments have also shown that thymocytes are able to maintain T cell production without the input of bone marrow progenitors for several weeks, a process called thymus autonomy (de Barros et al., 2013; Martins et al., 2012; Peaudecerf et al., 2012). However, although thymus autonomy has been associated with the development of T-ALL (Ballesteros-Arias et al., 2019; Martins et al., 2014) in mice, M-ATO-derived thymocytes maintained a highly diverse TCR Vβ repertoire without evidence of clonal outgrowth for at least 10 weeks of analysis.

The analysis of the TCR Vβ repertoire in M-ATO-derived thymocytes showed that some clones naturally eliminated in the thymus were present in M-ATOs, strongly suggesting that negative selection does not occur in the organoid system. This finding is consistent with the absence of thymic epithelial cells in ATOs. Although rare dendritic cells are detected in M-ATO cultures, their presence does not appear to be sufficient to induce negative selection. The detection of $GFP^+CD4^+CD25^+$ cells in M-ATOs generated from FOXP3-reporter mice is phenotypic evidence that Tregs are produced in M-ATOs, but definitive conclusions will require functional studies of these cells.

In the absence of thymic epithelium, positive selection of CD8SP cells is presumed to occur through MHC class I ligands ubiquitously presented by the stromal cells and the hematopoietic cells generated in the cultures. Monolayer murine co-cultures have not permitted the production of CD4SP cells, possibly because of a lack of class II expression or inefficiency of TCR-MHC interactions in these systems. The M-ATO system, however, clearly does generate CD4SP cells. Similar to human HSPC-derived ATOs (Seet et al., 2017), M-ATOs contain a population of hematopoietic cells that express MHC class II, though at a lower frequency than in the normal thymic microenvironment. It is interesting to note that M-ATOs seeded with hematopoietic populations with broad lineage (including myeloid) potential (HSC, MPP, and LMPP) readily generated CD4SP cells, whereas those initiated from progenitors with more restricted, lymphoid only potential (CLP and thymic progenitors) did not, supporting the idea that it is the presence of non-lymphoid lineages that provides the required class II presentation. It is also possible that the 3D structure of the ATO model provides more optimal interactions between MHC class II-expressing cells and T cell precursors than do monolayer systems; of note, other 3D systems (fetal thymic organ cultures and reaggregated primary stromal organoids) also allow positive selection and T cell maturation (Chung et al., 2014; Plum et al., 1994; Poznansky et al., 2000; Robinson and Owen, 1977). In addition, 3D structures may allow easier migration of maturing T cells away from Notch ligand-expressing stromal cells, a process that is seen during migration through the normal cortical-medullary thymic architecture. The M-ATO system offers a simple, reproducible, and modular platform to further explore the specific mechanisms of positive selection and the many other fundamental processes that drive T cell development.

STAR★METHODS

Detailed methods are provided in the online version of this paper and include the following:

RESOURCE AVAILABILITY

Lead Contact—Further information and requests for resources and reagents should be directed to and will be fulfilled by the lead Contact, Gay Crooks (gcrooks@mednet.ucla.edu).

Materials Availability—The MS5-mDLL4 cell lines generated in this study are available to academic investigators under an MTA with UCLA.

Data and Code Availability—The Gene Expression Omnibus (GEO) accession number for the RNA sequencing data reported in this paper is GEO: GSE146224. A detailed description of data analysis and the software used can be found in Method Details.

EXPERIMENTAL MODELS AND SUBJECT DETAILS

Cell lines—To generate MS5-mDLL4, MS5 cells (Itoh et al., 1989) were transduced with a lentiviral vector encoding full-length murine *DLL4* with or without enhanced green fluorescent protein (eGFP). The full-length coding sequence of murine *DLL4* was synthesized (Integrated DNA Technologies, Skokie, IL) and cloned into the third-generation lentiviral vector pCCL-c-MNDU3 (gift from Dr. Donald Kohn, UCLA) with or without IRES-linked eGFP expression. Packaging and concentration of lentivirus particles was performed as previously described (Seet et al., 2017). The highest 5% DLL4-expressing cells were sorted by FACS using an anti-DLL4 antibody (**Biolegend, Cat# 130813**) and passaged in Dulbecco's Modification of Eagle's Medium (DMEM) (**Cellgro, Cat# 10–017-CV**) 10% fetal calf serum (FCS) (**Gemini, Cat# 900–208**). Stable expression was confirmed by flow cytometry for DLL4 expression or GFP expression after several weeks of culture, as well as qRT-PCR and DNA sequencing.

Mice—All animal experiments were conducted under a protocol approved by the UCLA Chancellor's Animal Research Committee. This study used 1–4 month-old mice of different backgrounds from Jackson Laboratory (Bar Harbor, Maine): C57BL/6 (**Cat# JAX:000664**) (including Foxp3-GFP (**JAX:006772**) mice and RAG1$^{-/-}$ mice (**JAX:002216**)), C3H/He (**JAX:000659**), BALB/c (**JAX:000651**) and FVB (including Transgenic Notch Reporter mice (**JAX:020942**)) mice. Mice from both sexes were randomly allocated to experimental groups.

METHOD DETAILS

Isolation of murine bone marrow HSPCs—Fresh or frozen bone marrow cells were enriched for hematopoietic stem and progenitor cells by negative cells selection of Lin- cells by magnetic cell sorting (MACS) using Murine Lin depletion Kit (**Miltenyi, Auburn CA, Cat# 130–110-470**). Hematopoietic stem and progenitor cells were isolated by FACS sorting using the phenotypes as follow: (Lin$^-$ stands for: Ter119$^-$, TCR$\gamma\delta^-$, B220$^-$, CD19$^-$, CD11c$^-$, CD11b$^-$, Gr1$^-$, NK1.1$^-$, CD5$^-$, CD4$^-$, CD8$^-$, CD3$^-$).

Name of cell population	Phenotype
LSK (Lin^- $Sca1^+$ $cKit^+$)	Lin^- $Sca1^+$ $cKit^+$
HSC (Hematopoietic Stem Cell)	Lin^- $Sca1^+$ $cKit^+$ $CD48^-$ $CD150^+$ $IL7R^-$
MPP (MultiPotent Progenitor)	Lin^- $Sca1^+$ $cKit^+$ $CD48^-$ $CD150^-$ $IL7R^-$
LMPP (Lymphoid-primed MultiPotent Progenitor)	Lin^- $Sca1^+$ $cKit^+$ $IL7R^+$ $Flk2^+$
CLP (Common Lymphoid progenitor)	Lin^- $Sca1^{Lo}$ $cKit^{Lo}$ $IL7R^+$ $Flk2^+$

Sorted cells were immediately seeded into MS5-mDLL4 M-ATOs, as described below.

Murine artificial thymic organoid (M-ATO) cultures—M-ATOs were generated as previously described (Seet et al., 2017). MS5-mDLL4 cells were harvested by trypsinization and resuspended in serum free M-ATO culture medium (“D/F12-B27”) composed of DMEM-F12 (**GIBCO, Cat# 11320033**) (in some experiments, RPMI 1640 (**CellGro, Cat# 10–040-CV**) was used as basal media as indicated), 2% B27 supplement (**ThermoFisher Scientific, Grand Island, NY, Cat# 17504–044**) (in some experiments, 4% B27 was used as indicated), 30 μM L-ascorbic acid 2-phosphate sesquimagnesium salt hydrate (**Sigma-Aldrich, St. Louis, MO, Cat# A8960–5G**) reconstituted in PBS, 1% penicillin/streptomycin (**Gemini Bio-Products, West Sacramento, CA, Cat# 400–109**), 1% Glutamax (**ThermoFisher Scientific, Grand Island, NY, Cat# 35050–061**), 5 ng/ml rmFLT3L (**Peprotech, Rocky Hill, NJ, Cat# 250–31L**), 5 ng/ml rmIL-7 (**Peprotech, Cat# 217–17**), 10 ng/ml rmSCF (Peprotech, **Cat# 250–03**) (SCF was added only for the first week of culture) and beta mercaptoethanol (bME) (0.05mM) (**Sigma-Aldrich, Cat# M7522**). D/F12-B27 was made fresh weekly. 1.5×10^5 MS5-mDLL4 cells were combined with purified murine HSPC cells (1– 4000 cells / ATO) and centrifuged at 300 *g* for 5 min at 4°C in a swinging bucket centrifuge. Supernatants were carefully removed, and the cell pellet was resuspended in 5 μl D/F12-B27 per M-ATO and mixed by brief vortexing. M-ATOs were plated on a 0.4 μm Millicell transwell insert (**EMD Millipore, Billerica, MA; Cat. PICM0RG50**) placed in a 6-well plate containing 1 mL D/F12-B27 per well. Medium was changed completely every 3–4 days by aspiration from around the cell insert followed by replacement with 1 mL with fresh D/F12-B27/cytokines. M-ATO cells were harvested by adding FACS buffer (PBS/0.5% bovine serum album/2mM EDTA) to each well and briefly disaggregating the M-ATO by pipetting with a 1 mL “P1000” pipet, followed by passage through a 50 μm nylon strainer.

For single cell M-ATO cultures, LSK or HSC cells were isolated as single cells in a 96-conical bottom plate in 200ul of D/F12-B27 medium by flow cytometry cell sorting (FACS ARIA). After centrifugation, 1.5×10^5 MS5-mDLL4 cells were added in each well of the 96 well plate. The plate was then centrifuged at 300 *g* for 5 min at 4°C. Supernatants were carefully removed, and each cell pellet was resuspended in 5 μl D/F12-B27 and plated on a 0.4 μm Millicell transwell insert as described above.

Isolation of thymocytes and T cells—Thymic and spleen fragments from the mouse thymus were finely dissected in FACS buffer (PBS/0.5% bovine serum album/2mM EDTA)

and disrupted by pipetting to release thymocytes into suspension, followed by passage through a 70 μm nylon strainer. Cells were then stained for flow cytometry.

M-ATO-derived T cells were harvested by adding FACS buffer (PBS/0.5% bovine serum album/2mM EDTA) to each cell insert and briefly disaggregating the M-ATO by pipetting with a 1 mL “P1000” pipet, followed by passage through a 70 μm nylon strainer. Cells were then stained for flow cytometry.

Flow cytometry cell sorting of thymic and M-ATO-derived T cell populations used the following surface phenotypes: (Lin$^-$ stands here for: Ter119$^-$, TCRγδ$^-$, B220$^-$, CD19$^-$, CD11c$^-$, CD11b$^-$, Gr1$^-$, NK1.1$^-$).

Name of cell population	Phenotype
ETP (Early Thymic Progenitor)	Lin$^-$ CD4$^-$ CD8$^-$ c-Kit^{hi} CD44^{hi} CD25$^-$
DN2	Lin$^-$ CD4$^-$ CD8$^-$ c-Kit^{hi} CD44^{hi} CD25$^+$
DN3	Lin$^-$ CD4$^-$ CD8$^-$ CD44$^-$ CD25$^+$
ISP8	Lin$^-$ CD4$^-$ CD8$^+$ CD3$^-$
DP early	Lin$^-$ CD4$^+$ CD8$^+$ CD3$^-$ TCRβ$^-$
DP late	Lin$^-$ CD4$^+$ CD8$^+$ CD3$^+$ TCRβ$^+$
CD8SP	Lin$^-$ CD4$^-$ CD8$^+$ CD3$^+$ TCRβ$^+$ CD62L$^+$
CD4SP	Lin$^-$ CD4$^+$ CD8$^-$ CD3$^+$ TCRβ$^+$ CD62L$^+$

TCR Vβ expression analysis by flow cytometry—Total cells isolated from pooled M-ATOs or murine thymi were stained for Lin (Ter119, TCRγδ, B220, CD19, CD11c, CD11b, Gr1, NK1.1), CD3, CD4, CD8, in conjunction with the anti-mouse TCR Vβ Screening panel (**BD, Biosciences, Cat# 557004**). Lin$^-$CD3$^+$CD8$^+$CD4$^-$ cells and Lin$^-$ CD3$^+$CD8$^-$CD4$^+$ cells were gated for analysis, and Vβ family usage was determined by percent FITC$^+$, representing a different Vβ antibody per tube, per the manufacturer’s protocol.

T cell cytokine assays—Mature CD8SP and mature CD4SP cells from M-ATOs were isolated by magnetic negative selection using the CD8$^+$ T Cell Isolation Kit (**Miltenyi Biotech, Cat# 130–104-075**) and the CD4$^+$ T cell Isolation Kit (**Miltenyi Biotech, Cat# 130–104-454**) respectively and sorted by FACS or magnetic selection (**Miltenyi Biotech, Cat# 130–091-7558**) to further isolate CD8SP CD62L$^+$ cells and CD4SP CD62L$^+$ cells. Purified T cell populations were plated in 96-well U-bottom plates in 200 μl RPMI 1640 (**CellGro, Cat# 10–040-CV**) with 5% fetal calf serum (**Hyclone, Cat# SH30070.03**) and 0.05mM beta mercaptoethanol (bME) (**Sigma-Aldrich, Cat# M7522**). PMA/ionomycin/ protein transport inhibitor cocktail or control protein transport inhibitor cocktail (**eBioscience, San Diego, CA, Cat# 00–4975-03**) were added to each well and incubated for 6h. Cells were washed and stained for CD3, CD4, and CD8 (**Biolegend, San Diego, CA**) prior to fixation and permeabilization with an intracellular staining buffer kit (**eBioscience, San Diego, CA, Cat# 88–8824-00**) and intracellular staining with antibodies against IFNγ, TNFα, and IL-2 (**Biolegend, San Diego, CA**).

T cell activation and proliferation assays—For Cell Trace Violet (CTV) cell proliferation assays, M-ATO-derived CD8SP and CD4SP T cells were isolated as described above and labeled with 5 μM CTV (**Invitrogen, Cat# C34557**). Labeled cells were incubated with anti-CD3/CD28 beads per manufacturer's protocol (**ThermoFisher Scientific, Grand Island, NY, Cat# 11456D**) in RPMI 1640 (**CellGro, Cat# 10–040-CV**) with 5% fetal calf serum (**Hyclone, Cat# SH30070.03**) and 0.05mM beta mercaptoethanol (bME) (**Sigma-Aldrich, Cat# M7522**) with 20 ng/ml rmIL-2 (**Pepro-tech, Rocky Hill, NJ, Cat# 212–12**), and plated in 200 μl per well of 96-well round-bottom plates. On day 3, cells were washed and stained for CD25 (**Biolegend, San Diego, CA**) and analyzed by flow cytometry.

Immunofluorescence imaging of M-ATOs—M-ATOs were fixed in 4% Formaldehyde (**Sigma-Aldrich, Cat# F8775**) for 30 minutes at room temperature followed by 3×10 min washes in PBST (0.3% Triton X-100) and a 1-hour block in PBST/BSA (2% BSA). M-ATOs were stained with anti-CD8a (**clone 53–6.7; Biolegend**), anti-mDLL4 (**clone HMD4–1; Biolegend**), anti-CD4 (**clone RM4–5; Biolegend**), and anti-GFP (**clone FM264G; Biolegend**) at a 1:100 dilution, and anti-CD3 (**clone 145–2C11; Biolegend**) at a 1:50 dilution overnight at 4°C. Secondary antibodies AlexaFluor-594-conjugated anti-rat IgG (H+L) (**Jackson ImmunoResearch, Cat#** 712–585-150) or Alexa-Fluor-488-conjugated anti-rat IgG (H+L) (**Jackson ImmunoResearch, Cat# 712–485-153**) were added at a 1:200 dilution for 2 hours at room temperature. For anti-mDLL4, anti-hamster biotin (**Jackson ImmunoResearch, Cat# 127–065-160**) was added at a 1:500 dilution for 2 hours at room temperature, and then AlexaFluor-594-conjugated Streptavidin (**Jackson ImmunoResearch, Cat# 016–580-084**) was added at a 1:800 dilution for 30 minutes at room temperature. Each M-ATO was mounted individually in Vectashield Antifade Mounting Medium (**Vector Laboratories, Cat# H1000**) on a concavity microscope slide (**Fisher Scientific**). Immunofluo-rescence images were acquired on a Zeiss LSM 880 confocal microscope equipped with Airyscan and Zen software (**Zeiss**).

Flow cytometry—All flow cytometry stains were performed in PBS/0.5% BSA/2 mM EDTA for 20 min on ice. TruStain FcX (**Biolegend, San Diego, CA, Cat#101320**) was added to all samples for 5 min prior to antibody staining. DAPI (**Life technologies, Cat# D1306**) was added to all samples (except intracellular staining) prior to analysis.

For intracellular expression analysis, cells were stained for surface markers prior to fixation and permeabilization with the True-Nuclear Transcription Factor Buffer Set (**Biolegend, San Diego, CA, Cat# 424401**) followed by intracellular staining with antibodies.

Analysis was performed on an LSRII Fortessa, and FACS sorting on FACSARIA or FACSARIA-H instruments (**BD Biosciences, San Jose, CA**) at the UCLA Broad Stem Cell Research Center Flow Cytometry Core.

For all analyses (except intracellular staining) $DAPI^+$ cells were gated out, and single cells were gated based FSC-H versus FSC-W and SSC-H versus SSC-W.

Anti-mouse antibody clones used for surface and intracellular staining were obtained from Biolegend (San Diego, CA) or Miltenyi Biotech.

Flow cytometry antibody	SOURCE	IDENTIFIER
Anti-mouse CD3 (Clone145–2C11)	Biolegend	Cat# 100312, RRID:AB_312677
Anti-mouse CD4 (Clone RM4–5)	Biolegend	Cat# 100550, RRID:AB_2562099
Anti-mouse CD5 (Clone 53–7.3)	Biolegend	Cat# 100627, RRID:AB_2563930
Anti-mouse CD8a (Clone 53–6.7)	Biolegend	Cat# 100708, RRID:AB_312747
Anti-mouse CD11b (Clone M1/70)	Biolegend	Cat# 101228, RRID:AB_893232
Anti-mouse CD11c (Clone N418)	Biolegend	Cat# 117328, RRID:AB_2129641
Anti-mouse CD16/32 (TruStain FcX) (Clone 93)	Biolegend	Cat# 101320, RRID:AB_1574975
Anti-mouse CD19 (Clone 1D3/CD19)	Biolegend	Cat# 152406, RRID:AB_2629815
Anti-mouse CD25 (PC61)	Biolegend	Cat# 102016, RRID:AB_312865
Anti-mouse CD27 (LG.3A10)	Biolegend	Cat# 124226, RRID:AB_2565792
Anti-mouse CD28 (37.5)	Biolegend	Cat# 102127, RRID:AB_2650628
Anti-mouse CD44 (IM7)	Biolegend	Cat# 103059, RRID:AB_2571953
Anti-mouse CD45 (clone 30-F11)	Biolegend	Cat# 103116, RRID:AB_312981
Anti-mouse CD45R/B220 (Clone RA3–6B2)	Biolegend	Cat# 103236, RRID:AB_893354
Anti-mouse CD62L (MEL-14)	Biolegend	Cat# 104438, RRID:AB_2563058
Anti-mouse Ly-6G/Ly-6C (Gr-1) (Clone RB6–8C5)	Biolegend	Cat# 108428, RRID:AB_893558
Anti-mouse NK1.1 (Clone PK136)	Biolegend	Cat# 108728, RRID:AB_2132705
Anti-mouse interferon γ (Clone XMG1.2)	Biolegend	Cat# 505806, RRID:AB_315400
Anti-mouse IL-2 (Clone JES6–5H4)	Biolegend	Cat# 503826, RRID:AB_2650897
Anti-mouse TCRβ (Clone H57–597)	Biolegend	Cat# 109234, RRID:AB_2562350
Anti-mouse TCRγδ (Clone GL3)	Biolegend	Cat# 118120, RRID:AB_2562566
Anti-mouse TNFα (Clone MP6-XT22)	Biolegend	Cat# 506339, RRID:AB_2563127
Anti-mouse TER-119 (clone Ter119)	Biolegend	Cat# 116228, RRID:AB_893636
Anti-mouse CD150 (Clone TC15–12F12.2)	Biolegend	Cat# 115941, RRID:AB_2629660
Anti-mouse CD117 (c-KIT) (Clone ACK2)	Biolegend	Cat# 135122, RRID:AB_2562042
Anti-mouse Ly-6A/E (Sca-1) (Clone D7)	Biolegend	Cat# 108114, RRID:AB_493596
Anti-mouse CD48 (Clone HM48–1)	Biolegend	Cat# 103432, RRID:AB_2561463
Anti-mouse CD127 (IL-7R) (Clone REA680)	Miltenyi Biotech	Cat# 130–122-938, RRID:AB_2783928
Anti-mouse CD135 (Flk-2) (Clone A2F10)	Biolegend	Cat# 135306, RRID:AB_1877217
Anti-mDLL4 (clone HMD4–1)	Biolegend	Cat# 130813, RRID:AB_2246026

Flow cytometry data were analyzed with FlowJo software (**Tree Star Inc**.).

RNA sequencing (RNA-seq) and data analysis—RNA was extracted from each of the indicated Thymic or M-ATO-derived populations isolated by FACS, as described above, and total RNA isolated using the RNeasy Micro kit (QIAGEN). (Lin^- stands here for: $Ter119^-$, $TCR\gamma\delta^-$, $B220^-$, $CD19^-$, $CD11c^-$, $CD11b^-$, $Gr1^-$, $NK1.1^-$).

Name of cell population	Number of replicates (n)	Phenotype
ETP thymus	2	Lin^- $CD4^-$ $CD8^-$ c-Kit^{hi} $CD44^{hi}$ $CD25^-$
ETP M-ATO	2	Lin^- $CD4^-$ $CD8^-$ c-Kit^{hi} $CD44^{hi}$ $CD25^-$
DN2 thymus	2	Lin^- $CD4^-$ $CD8^-$ c-Kit^{hi} $CD44^{hi}$ $CD25^+$
DN2 M-ATO	2	Lin^- $CD4^-$ $CD8^-$ c-Kit^{hi} $CD44^{hi}$ $CD25^+$
DN3 thymus	2	Lin^- $CD4^-$ $CD8^-$ $CD44^-$ $CD25^+$
DN3 M-ATO	2	Lin^- $CD4^-$ $CD8^-$ $CD44^-$ $CD25^+$
ISP8 thymus	2	Lin^- $CD4^-$ $CD8^+$ $CD3^-$
ISP8 M-ATO	2	Lin^- $CD4^-$ $CD8^+$ $CD3^-$
DP early thymus	2	Lin^- $CD4^+$ $CD8^+$ $CD3^-$ $TCR\beta^-$
DP early M-ATO	2	Lin^- $CD4^+$ $CD8^+$ $CD3^-$ $TCR\beta^-$
DP late thymus	2	Lin^- $CD4^+$ $CD8^+$ $CD3^+$ $TCR\beta^+$
DP late M-ATO	2	Lin^- $CD4^+$ $CD8^+$ $CD3^+$ $TCR\beta^+$
CD8SP thymus	2	Lin^- $CD4^-$ $CD8^+$ $CD3^+$ $TCR\beta^+$ $CD62L^+$
CD8SP M-ATO	2	Lin^- $CD4^-$ $CD8^+$ $CD3^+$ $TCR\beta^+$ $CD62L^+$
CD4SP thymus	2	Lin^- $CD4^+$ $CD8^-$ $CD3^+$ $TCR\beta^+$ $CD62L^+$
CD4SP M-ATO	2	Lin^- $CD4^+$ $CD8^-$ $CD3^+$ $TCR\beta^+$ $CD62L^+$

1.5 ng of total RNA was input to generate sequencing libraries with SMARTer Stranded Total RNA-Seq (Pico) Kit (Clonetech, Cat. 635005). Paired-end 150 bp sequencing was performed on an Illumina HiSeq 3000. A total of 32 libraries were multiplexed and sequenced in 5 lanes. Raw sequence files are available at NCBI's Gene Expression Omnibus (GSE146224). An independent set of RNA-Seq libraries for thymic subsets generated by the Immgen consortium (GSE127267) was downloaded from NCBI's Gene Expression Omnibus (Bioproject ID PRJNA429735) and analyzed in-house (Table S1).

The STAR ultrafast universal RNA-seq aligner v2.7.0d (Dobin et al., 2013) was used to align the reads to a genome index that includes both the genome sequence (GRCm38 mouse primary assembly) and the exon/intron structure of known mouse gene models (Gencode M20 comprehensive genome annotation). Alignment files were used to generate strand-specific, gene-level count summaries with STAR's built-in gene counter. Data from the Immgen dataset was not strand-specific. Independent filtering was applied as follows: genes with less than half-count per million in all samples, count outliers or low mappability (< 50bp) were filtered out for downstream analysis (Casero et al., 2015; Love et al., 2014). This masked set included a total of 13760 mouse protein coding genes.

Expression estimates provided throughout were computed in units of fragments per kilobase of mappable length and million counts (FPKMs). Count-based normalized and variance-stabilized data were used for all ordination, differential, and clustering analyses, and all figures unless otherwise noted.

Principal component analysis (PCA, Figures 4A and 4B) was performed with the function prcomp in R (https://www.R-project.org/) using standardize data as input. To facilitate the

integration of in-house and external datasets, standardization was performed independently prior to PCA.

Differential expression analyses was performed with DESeq2 (Bioconductor, v3.7, RRID:SCR_015687) (Love et al., 2014). We performed pairwise comparisons between and within thymocyte subsets from both thymic and M-ATO. We defined a set of 2554 variable genes for further analyses as: fold-change greater than 4, Benjamini-Hochberg adjusted Wald test p value less than 0.01 in at least one pairwise test, and a minimum expression of 4 FPKMs in at least one sample. This set of most variable genes was then subjected to model-based clustering using MBCluster.Seq (Si et al., 2014) to classify them based on their overall abundance profile across populations (Figures 4C and 4D). We set the starting number of clusters to 100, and then manually merged them to generate a set of 26 non-redundant gene classes (Table S1).

Functional enrichment for genes selected in the tests and clusters above was performed with Metascape (Zhou et al., 2019).

Fold changes between two developmentally proximal populations were employed to perform Gene Set Enrichment Analysis (Subramanian et al., 2005) using gene expression signatures from independent studies (Figure S4). We analyzed the following transitions in both M-ATO-derived and thymic populations from this study: the *ETP/DN2* transition from our samples was compared against the “ETP < DN2” (higher expression in DN2) and “ETP > DN2” (higher expression in ETP) signatures from the Molecular Signature Database (MSigDB) and similarly for *DN2/DN3* (MSigDB: DN2 > DN3, DN2 < DN3). For the *ISP/DPearly* transition we employed a signature for the most regulated genes between double negative and double positive cells (MSigDB: DN > DP, DN < DP). For the *DPlate/CD4SP* and *DPlate/CD8SP* transitions we retrieved a signature from the Immgen microarray database (Mingueneau et al., 2013) with genes most differential between $DP69^+$ cells (double positive $CD69^+$ cells, early positive selection) and $4SP24^-$ ($CD4^+$ single positive $CD24^-$mature T cells) or $8SP24^-$ ($CD8^+$ single positive $CD24^-$ mature T cells) respectively. Finally, the divergence between our *CD4SP* and *CD8SP* single positive populations in both M-ATOs and thymus was compared against a signature from the $4SP24^-$ versus $8SP24^-$ mature thymic T cells contrast from Immgen. Each of the previous signatures typically included a list of the 150 to 200 most up- or downregulated genes between any two populations. All plots in Figures 4 and S4 were generated in MATLAB (MATLAB, version release 2017a, The MathWorks, Inc, RRID:SCR_001622).

QUANTIFICATION AND STATISTICAL ANALYSIS

In all figures, *n* represents independent experiments and data are represented as mean ± standard deviation (SD) or mean ± standard error of the mean (SEM) as indicated. Statistical analysis was performed using GraphPad Prism software and *p-value*s were calculated from the two-tailed unpaired t test or multiple t test. The *p-value*s are directly indicated on the figure, above the corresponding graphs. *p < 0.05; **p < 0.01; and ***p < 0.001 were considered statistically significant.

Supplementary Material

Refer to Web version on PubMed Central for supplementary material.

ACKNOWLEDGMENTS

We gratefully acknowledge the expert technical assistance of Felicia Codrea, Jessica Scholes, and Jeffrey Calimlim from the UCLA Broad Stem Cell Research Center (BSCRC) Flow Cytometry Core, as well as the Technology Center for Genomics and Bioinformatics (TCGB) at UCLA and the Translational Pathology Core Laboratory (TPCL) at UCLA. We thank L. Coulombel for generously providing us with MS-5 cells many years ago. This work was supported by National Institutes of Health (NIH) grants RO1AG049753 and R21AI119927 (G.M.C.); 5P30AG028748/UL1TR000124 (National Center for Advancing Translational Sciences [NCATS]/UCLA Clinical and Translational Science Institute [CTSI]) (D.C.); P30CA016042 (National Cancer Institute [NCI]) (TCGB and TPCL cores), KL2TR001882 (NIH/NCATS/UCLA CTSI), and K08CA235525 (NIH/NCI) (C.S.S.); NIH T32GM008042 (V.S.); and the Connie Frank and Evan Thompson Program for Collaborative Restorative Transplantation Research. V.S. acknowledges the support of the Eli and Edythe Broad Center of Regenerative Medicine and Stem Cell Research at UCLA Training Program.

REFERENCES

Abe R, Kanagawa O, Sheard MA, Malissen B, and Foo-Phillips M. (1991). Characterization of a new minor lymphocyte stimulatory system. I. Cluster of self antigens recognized by “I-E-reactive” V beta s, V beta 5, V beta 11, and V beta 12 T cell receptors for antigen. J. Immunol. 147, 739–749. [PubMed: 1713604]

Ballesteros-Arias L, Silva JG, Paiva RA, Carbonetto B, Faísca P, and Martins VC (2019). T cell acute lymphoblastic leukemia as a consequence of thymus autonomy. J. Immunol. 202, 1137–1144. [PubMed: 30651344]

Berzins SP, Boyd RL, and Miller JFAP (1998). The role of the thymus and recent thymic migrants in the maintenance of the adult peripheral lymphocyte pool. J. Exp. Med. 187, 1839–1848. [PubMed: 9607924]

Bill J, Kanagawa O, Woodland DL, and Palmer E. (1989). The MHC molecule I-E is necessary but not sufficient for the clonal deletion of V beta 11-bearing T cells. J. Exp. Med. 169, 1405–1419. [PubMed: 2538552]

Bill J, Kanagawa O, Linten J, Utsunomiya Y, and Palmer E. (1990). Class I and class II MHC gene products differentially affect the fate of V beta 5 bearing thymocytes. J. Mol. Cell. Immunol. 4, 269–279, discussion 279–280. [PubMed: 1976311]

Boehm T. (2012). Self-renewal of thymocytes in the absence of competitive precursor replenishment. J. Exp. Med. 209, 1397–1400. [PubMed: 22851642]

Bradley LM, Watson SR, and Swain SL (1994). Entry of naive CD4 T cells into peripheral lymph nodes requires L-selectin. J. Exp. Med. 180, 2401–2406. [PubMed: 7525854]

Brandt D, and Hedrich CM (2018). TCRαβ+CD3+CD4-CD8- (double negative) T cells in autoimmunity. Autoimmun. Rev. 17, 422–430. [PubMed: 29428806]

Breed ER, Lee ST, and Hogquist KA (2018). Directing T cell fate: how thymic antigen presenting cells coordinate thymocyte selection. Semin. Cell Dev. Biol. 84, 2–10. [PubMed: 28800929]

Budd RC, Cerottini JC, Horvath C, Bron C, Pedrazzini T, Howe RC, and MacDonald HR (1987). Distinction of virgin and memory T lymphocytes. Stable acquisition of the Pgp-1 glycoprotein concomitant with antigenic stimulation. J. Immunol. 138, 3120–3129. [PubMed: 3106474]

Casero D, Sandoval S, Seet CS, Scholes J, Zhu Y, Ha VL, Luong A, Parekh C, and Crooks GM (2015). Long non-coding RNA profiling of human lymphoid progenitor cells reveals transcriptional divergence of B cell and T cell lineages. Nat. Immunol. 16, 1282–1291. [PubMed: 26502406]

Chung B, Montel-Hagen A, Ge S, Blumberg G, Kim K, Klein S, Zhu Y, Parekh C, Balamurugan A, Yang OO, and Crooks GM (2014). Engineering the human thymic microenvironment to support thymopoiesis in vivo. Stem Cells 32, 2386–2396. [PubMed: 24801626]

de Barros SC, Vicente R, Chebli K, Jacquet C, Zimmermann VS, and Taylor N. (2013). Intrathymic progenitor cell transplantation across histocompatibility barriers results in the persistence of early thymic progenitors and T-cell differentiation. Blood 121, 2144–2153. [PubMed: 23305740]

Dobin A, Davis CA, Schlesinger F, Drenkow J, Zaleski C, Jha S, Batut P, Chaisson M, and Gingeras TR (2013). STAR: ultrafast universal RNA-seq aligner. Bioinformatics 29, 15–21. [PubMed: 23104886]

Fan Y, Tajima A, Goh SK, Geng X, Gualtierotti G, Grupillo M, Coppola A, Bertera S, Rudert WA, Banerjee I, et al. (2015). Bioengineering thymus organoids to restore thymic function and induce donor-specific immune tolerance to allografts. Mol. Ther. 23, 1262–1277. [PubMed: 25903472]

Fontenot JD, Rasmussen JP, Williams LM, Dooley JL, Farr AG, and Rudensky AY (2005). Regulatory T cell lineage specification by the forkhead transcription factor foxp3. Immunity 22, 329–341. [PubMed: 15780990]

Gao EK, Kanagawa O, and Sprent J. (1989). Capacity of unprimed CD4+ and CD8+ T cells expressing V beta 11 receptors to respond to I-E alloantigens in vivo. J. Exp. Med. 170, 1947–1957. [PubMed: 2531192]

Godfrey DI, Kennedy J, Suda T, and Zlotnik A. (1993). A developmental pathway involving four phenotypically and functionally distinct subsets of CD3-CD4-CD8- triple-negative adult mouse thymocytes defined by CD44 and CD25 expression. J. Immunol. 150, 4244–4252. [PubMed: 8387091]

Hare KJ, Jenkinson EJ, and Anderson G. (1999). In vitro models of T cell development. Semin. Immunol. 11, 3–12. [PubMed: 9950748]

Hodes RJ, and Abe R. (2001). Mouse endogenous superantigens: Ms and Mls-like determinants encoded by mouse retroviruses. Curr Protoc Immunol Appendix 1 (Appendix), 1F.

Hozumi K, Mailhos C, Negishi N, Hirano K, Yahata T, Ando K, Zuklys S, Holländer GA, Shima DT, and Habu S. (2008). Delta-like 4 is indispensable in thymic environment specific for T cell development. J. Exp. Med. 205, 2507–2513. [PubMed: 18824583]

Itoh K, Tezuka H, Sakoda H, Konno M, Nagata K, Uchiyama T, Uchino H, and Mori KJ (1989). Reproducible establishment of hemopoietic supportive stromal cell lines from murine bone marrow. Exp. Hematol. 17, 145–153. [PubMed: 2783573]

Koch U, Fiorini E, Benedito R, Besseyrias V, Schuster-Gossler K, Pierres M, Manley NR, Duarte A, Macdonald HR, and Radtke F. (2008). Delta-like 4 is the essential, nonredundant ligand for Notch1 during thymic T cell lineage commitment. J. Exp. Med. 205, 2515–2523. [PubMed: 18824585]

Ley K, and Tedder TF (1995). Leukocyte interactions with vascular endothelium. New insights into selectin-mediated attachment and rolling. J. Immunol. 155, 525–528. [PubMed: 7541818]

Lio C-WJ, and Hsieh C-S (2008). A two-step process for thymic regulatory T cell development. Immunity 28, 100–111. [PubMed: 18199417]

Love PE, and Bhandoola A. (2011). Signal integration and crosstalk during thymocyte migration and emigration. Nat. Rev. Immunol. 11, 469–477. [PubMed: 21701522]

Love MI, Huber W, and Anders S. (2014). Moderated estimation of fold change and dispersion for RNA-seq data with DESeq2. Genome Biol. 15, 550. [PubMed: 25516281]

Marshall D, Sinclair C, Tung S, and Seddon B. (2014). Differential requirement for IL-2 and IL-15 during bifurcated development of thymic regulatory T cells. J. Immunol. 193, 5525–5533. [PubMed: 25348623]

Martins VC, Ruggiero E, Schlenner SM, Madan V, Schmidt M, Fink PJ, von Kalle C, and Rodewald H-R (2012). Thymus-autonomous T cell development in the absence of progenitor import. J. Exp. Med. 209, 1409–1417. [PubMed: 22778389]

Martins VC, Busch K, Juraeva D, Blum C, Ludwig C, Rasche V, Lasitschka F, Mastitsky SE, Brors B, Hielscher T, et al. (2014). Cell competition is a tumour suppressor mechanism in the thymus. Nature 509, 465–470. [PubMed: 24828041]

Mingueneau M, Kreslavsky T, Gray D, Heng T, Cruse R, Ericson J, Bendall S, Spitzer MH, Nolan GP, Kobayashi K, et al.; Immunological Genome Consortium (2013). The transcriptional landscape of αβ T cell differentiation. Nat. Immunol. 14, 619–632. [PubMed: 23644507]

Mombaerts P, Iacomini J, Johnson RS, Herrup K, Tonegawa S, and Papaioannou VE (1992). RAG-1-deficient mice have no mature B and T lymphocytes. Cell 68, 869–877. [PubMed: 1547488]

Montel-Hagen A, Seet CS, Li S, Chick B, Zhu Y, Chang P, Tsai S, Sun V, Lopez S, Chen H-C, et al. (2019). Organoid-induced differentiation of conventional T cells from human pluripotent stem cells. Cell Stem Cell 24, 376–389.e8. [PubMed: 30661959]

Nowotschin S, Xenopoulos P, Schrode N, and Hadjantonakis A-K (2013). A bright single-cell resolution live imaging reporter of Notch signaling in the mouse. BMC Dev. Biol. 13, 15. [PubMed: 23617465]

Peaudecerf L, Lemos S, Galgano A, Krenn G, Vasseur F, Di Santo JP, Ezine S, and Rocha B. (2012). Thymocytes may persist and differentiate without any input from bone marrow progenitors. J. Exp. Med. 209, 1401–1408. [PubMed: 22778388]

Petkova SB, Yuan R, Tsaih S-W, Schott W, Roopenian DC, and Paigen B. (2008). Genetic influence on immune phenotype revealed strain-specific variations in peripheral blood lineages. Physiol. Genomics 34, 304–314. [PubMed: 18544662]

Plum J, De Smedt M, Defresne MP, Leclercq G, and Vandekerckhove B. (1994). Human CD34+ fetal liver stem cells differentiate to T cells in a mouse thymic microenvironment. Blood 84, 1587–1593. [PubMed: 7520780]

Poznansky MC, Evans RH, Foxall RB, Olszak IT, Piascik AH, Hartman KE, Brander C, Meyer TH, Pykett MJ, Chabner KT, et al. (2000). Efficient generation of human T cells from a tissue-engineered thymic organoid. Nat. Biotechnol. 18, 729–734. [PubMed: 10888839]

Robinson JH, and Owen JJ (1977). Generation of T-cell function in organ culture of foetal mouse thymus. II. Mixed lymphocyte culture reactivity. Clin. Exp. Immunol. 27, 322–327. [PubMed: 139222]

Rothenberg EV (2011). T cell lineage commitment: identity and renunciation. J. Immunol. 186, 6649–6655. [PubMed: 21646301]

Rothenberg EV (2019). Programming for T-lymphocyte fates: modularity and mechanisms. Genes Dev. 33, 1117–1135. [PubMed: 31481536]

Rothenberg EV, Moore JE, and Yui MA (2008). Launching the T-cell-line-age developmental programme. Nat. Rev. Immunol. 8, 9–21. [PubMed: 18097446]

Schmitt TM, and Zúñiga-Pflücker JC (2002). Induction of T cell development from hematopoietic progenitor cells by delta-like-1 in vitro. Immunity 17, 749–756. [PubMed: 12479821]

Seet CS, He C, Bethune MT, Li S, Chick B, Gschweng EH, Zhu Y, Kim K, Kohn DB, Baltimore D, et al. (2017). Generation of mature T cells from human hematopoietic stem and progenitor cells in artificial thymic organoids. Nat. Methods 14, 521–530. [PubMed: 28369043]

Shannon P, Markiel A, Ozier O, Baliga NS, Wang JT, Ramage D, Amin N, Schwikowski B, and Ideker T. (2003). Cytoscape: A software environment for integrated models of biomolecular interaction networks. Genome 13, 2498–2504.

Si Y, Liu P, Li P, and Brutnell TP (2014). Model-based clustering for RNA-seq data. Bioinformatics 30, 197–205. [PubMed: 24191069]

Subramanian A, Tamayo P, Mootha VK, Mukherjee S, Ebert BL, Gillette MA, Paulovich A, Pomeroy SL, Golub TR, Lander ES, and Mesirov JP (2005). Gene set enrichment analysis: a knowledge-based approach for interpreting genome-wide expression profiles. Proc. Natl. Acad. Sci. U S A 102, 15545–15550. [PubMed: 16199517]

Sugihara S, Maruo S, Tsujimura T, Tarutani O, Kohno Y, Hamaoka T, and Fujiwara H. (1990). Autoimmune thyroiditis induced in mice depleted of particular T cell subsets. III. Analysis of regulatory cells suppressing the induction of thyroiditis. Int. Immunol. 2, 343–351. [PubMed: 2149064]

Taghon T, Yui MA, Pant R, Diamond RA, and Rothenberg EV (2006). Developmental and molecular characterization of emerging beta- and gamma-delta-selected pre-T cells in the adult mouse thymus. Immunity 24, 53–64. [PubMed: 16413923]

Tai X, Erman B, Alag A, Mu J, Kimura M, Katz G, Guinter T, McCaughtry T, Etzensperger R, Feigenbaum L, et al. (2013). Foxp3 transcription factor is proapoptotic and lethal to developing regulatory T cells unless counter-balanced by cytokine survival signals. Immunity 38, 1116–1128. [PubMed: 23746651]

Takahama Y. (2006). Journey through the thymus: stromal guides for T-cell development and selection. Nat. Rev. Immunol. 6, 127–135. [PubMed: 16491137]

Teague TK, Tan C, Marino JH, Davis BK, Taylor AA, Huey RW, and Van De Wiele CJ (2010). CD28 expression redefines thymocyte development during the pre-T to DP transition. Int. Immunol. 22, 387–397. [PubMed: 20203098]

Tomonari K, Fairchild S, and Rosenwasser OA (1993). Influence of viral superantigens on V beta- and V alpha-specific positive and negative selection. Immunol. Rev. 131, 131–168. [PubMed: 8387455]

Vacchio MS, and Hodes RJ (1989). Selective decreases in T cell receptor V beta expression. Decreased expression of specific V beta families is associated with expression of multiple MHC and non-MHC gene products. J. Exp. Med. 170, 1335–1346. [PubMed: 2529341]

Wilson A, Capone M, and MacDonald HR (1999). Unexpectedly late expression of intracellular CD3epsilon and TCR gammadelta proteins during adult thymus development. Int. Immunol. 11, 1641–1650. [PubMed: 10508182]

Woodland D, Happ MP, Bill J, and Palmer E. (1990). Requirement for cotolerogenic gene products in the clonal deletion of I-E reactive T cells. Science 247, 964–967. [PubMed: 1968289]

Woodland DL, Happ MP, Gollob KJ, and Palmer E. (1991). An endogenous retrovirus mediating deletion of alpha beta T cells? Nature 349, 529–530. [PubMed: 1846949]

Yamamoto R, Xu Yan, Ikeda S, Sumida K, Tanaka H, Hozumi K, Takaori-Kondo A, and Minato N. (2019). Thymic development of a unique bone marrow–resident innate-like T cell subset with a potent innate immune function. J. Immunol. 203, 167–177. [PubMed: 31085589]

Yui MA, Feng N, and Rothenberg EV (2010). Fine-scale staging of T cell lineage commitment in adult mouse thymus. J. Immunol. 185, 284–293. [PubMed: 20543111]

Zhou Y, Zhou B, Pache L, Chang M, Khodabakhshi AH, Tanaseichuk O, Benner C, and Chanda SK (2019). Metascape provides a biologist-oriented resource for the analysis of systems-level datasets. Nat. Commun. 10, 1523. [PubMed: 30944313]

Highlights

- M-ATOs mimic the different stages of normal murine thymopoiesis in multiple strains
- M-ATOs support the key transcriptional transitions during T cell development
- M-ATOs generate mature T cells with a diverse TCR repertoire
- M-ATOs generate the complete trajectory of thymopoiesis from a single HSC

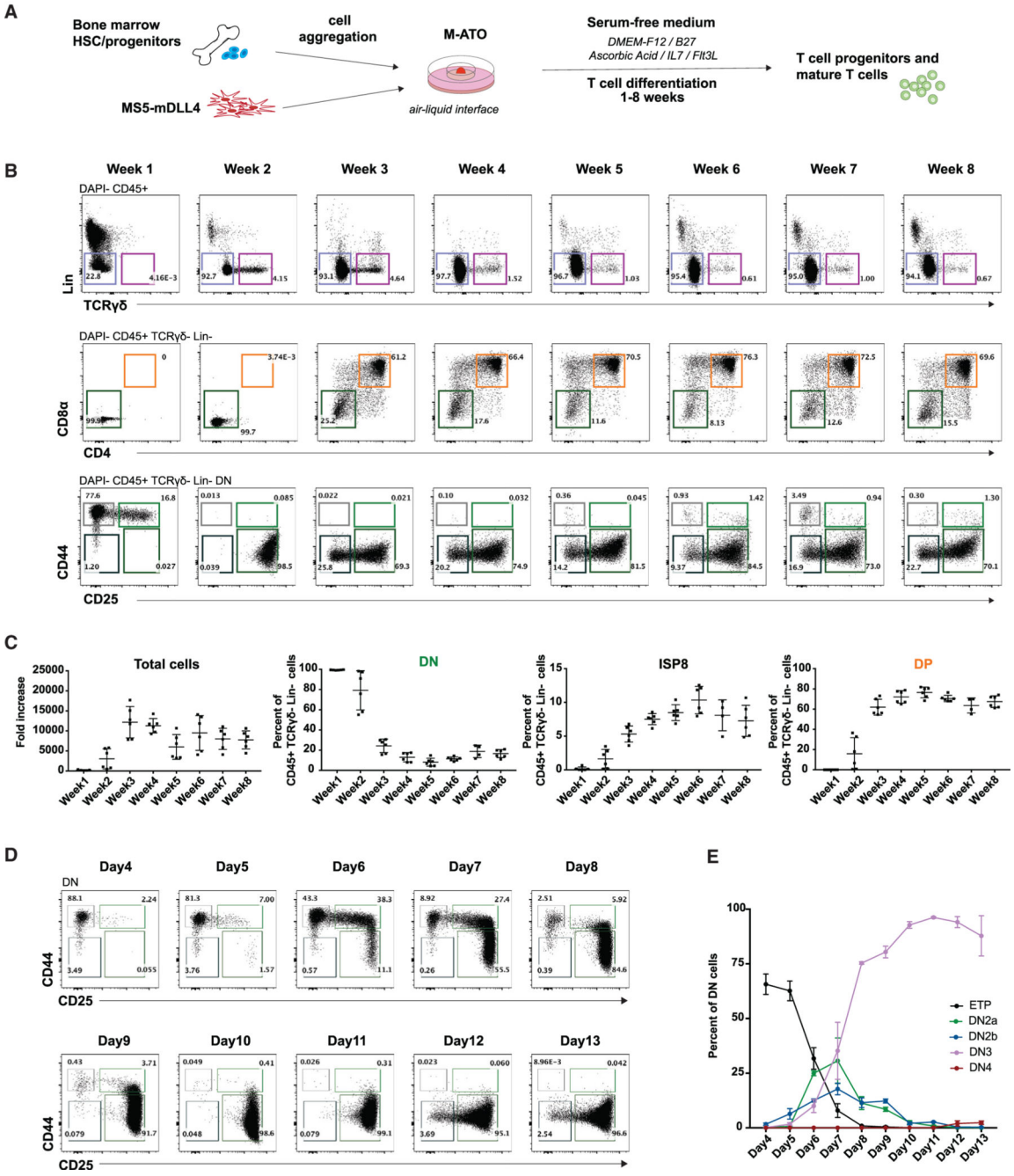

Figure 1. Kinetics of Early T Cell Differentiation in Murine ATOs

(A) Schematic of the M-ATO system.

(B) Representative kinetic analysis of T cell differentiation from bone marrow lineage-negative, Sca1^{+}, cKit^{+} (LSK) isolated from C57BL/6 wild-type (WT) mice at the indicated time points, gated on CD45^{+} cells to exclude non-hematopoietic cells. Middle and bottom rows: cells are gated on CD11b^{-}, CD11c^{-}, Gr1^{-}, CD19^{-}, B220^{-}, and NK1.1^{-} (Lin neg) and TCR$\gamma\delta^{-}$ cells. Bottom row: cells are further gated on double-negative (DN) cells CD8^{-}

$CD4^-$ to analyze DN subsets: DN1 ($CD44^+CD25^-$), DN2 ($CD44^+CD25^+$), DN3 ($CD44^-CD25^+$), and DN4 ($CD44^-CD25^-$) (Figure S1C).

(C) Fold increase and frequencies of cell populations in M-ATOs over time. Left graph shows fold increase in total cell number from LSK cells seeded in M-ATOs at day 0. Frequencies of DN cells ($CD8^-CD4^-$), immature single-positive $CD8^+$ (ISP8) cells ($CD8^+CD4^-CD3^-$), and double-positive (DP) cells ($CD8^+CD4^+$) are shown as percentage of total $CD45^+$ TCR$\gamma\delta^-$ Lin^- cells. Error bar denotes ±SD (n = 6 independent experiments).

(D) Representative kinetic analysis of early T cell development within the DN population during the first 2 weeks of culture in M-ATOs.

(E) Frequencies of early T cell populations over the first 2 weeks in M-ATOs. Frequencies of early thymic progenitors (ETPs) ($ckit^{Hi}$, $CD44^+CD25^-$), DN2a ($ckit^{Hi}$, $CD44^+CD25^+$), DN2b ($ckit^{med}$, $CD44^+CD25^+$), DN3 ($CD44^-CD25^+$), and DN4 ($CD44^-CD25^-$) are shown as percentage of total DN cells. Error bar denotes ±SD (n = 3 independent experiments).

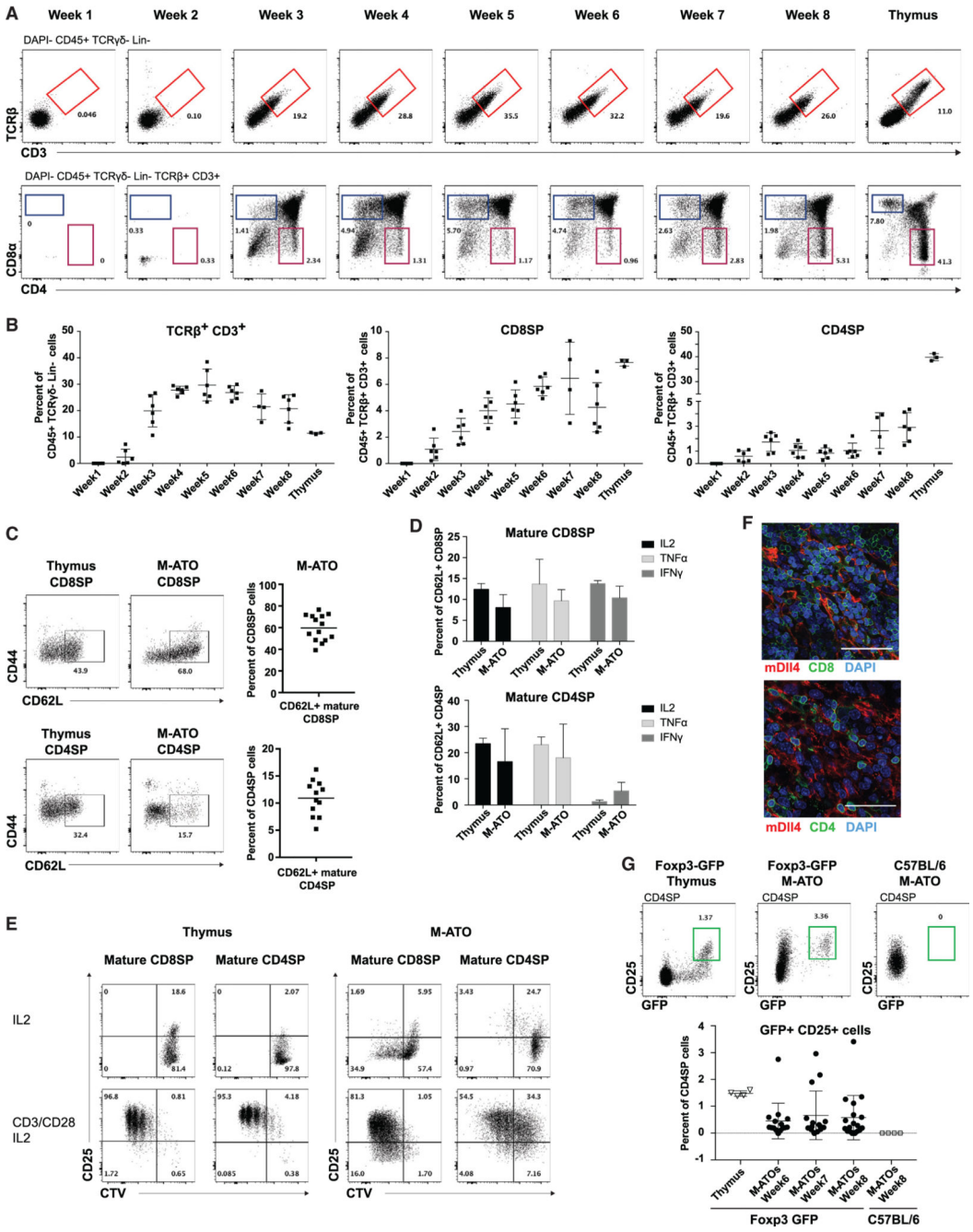

Figure 2. Murine ATOs Generate Functional CD8SP and CD4SP Mature T Cells and Foxp3^{+} CD4^{+} Treg-like Cells

(A) Representative kinetic analysis of T cell maturation from LSK cells isolated from C57BL/6 WT mice at the indicated time points gated on CD45^{+} TCRγδ^{-} Lin^{-}. CD4 and CD8 mature single-positive cells (CD4SP and CD8SP respectively) are gated on TCRβ^{+} CD3^{+} cells (bottom row).

(B) Frequencies of TCRβ^{+} CD3^{+} cells (left) are shown as percentage of total CD45^{+} TCRγδ^{-} Lin^{-} cells; CD8SP cells (CD8^{+} CD4^{-} CD3^{+} TCRβ^{+}) (middle) and CD4SP cells (CD8^{-} CD4^{+} CD3^{+} TCRβ^{+}) (right) are shown as percentage of CD45^{+} TCRβ^{+} CD3^{+} cells in M-

ATOs and in the thymus. Error bar denotes ±SD (M-ATO, n = 6 independent experiments; thymus, n = 3).

(C) Expression of the maturation marker CD62L on CD8SP and CD4SP cells in week 7 M-ATOs. Summary of data on CD62L expression shown as percentage of CD8SP and CD4SP (n = 12 independent M-ATOSs). Frequencies of $CD62L^+$ and naive CD4SP (CD4SP $CD62L^+$) are shown as percentage of CD8SP and CD4SP, respectively (n = 12 independent M-ATOs).

(D) Polyfunctional cytokine production by thymic or M-ATO-derived $CD62L^+$ CD8SP (top) and $CD62L^+$ CD4SP (bottom) after treatment with PMA + ionomycin for 6 h. Error bar denotes ± SEM (thymus SP8 and SP4, n = 2; M-ATO SP8, n = 5; M-ATO SP4, n = 2).

(E) Proliferation (as measured by dilution of CellTrace Violet (CTV) and activation (upregulation of CD25) of thymic (left) and M-ATO-derived (right) $CD62L^+$ CD8SP and $CD62L^+$ CD4SP after 3 days of treatment with IL2 ± anti-CD3/CD28 stimulation. Data are representative of three independent experiments.

(F) Representative immunofluorescence analysis (n = 3) for CD8 (green) and mDLL4 (red) expression (upper) and CD4 (green) and mDLL4 (red) (lower) in week 4 M-ATOs. Nuclei were stained with DAPI. Scale bars, 50 μm.

(G) GFP expression in CD4SP cells from thymocytes harvested from the Foxp3-GFP reporter mouse (left), generated in week 7 M-ATOs from LSK cells isolated from Foxp3-GFP (middle) or C57BL/6 WT mice (right). Frequencies of $Foxp3^+$ $CD25^+$ Treg-like T cells are shown as percentage of total CD4SP T cells in thymus (n = 4) or in M-ATOs over time (n = 15 independent M-ATOs).

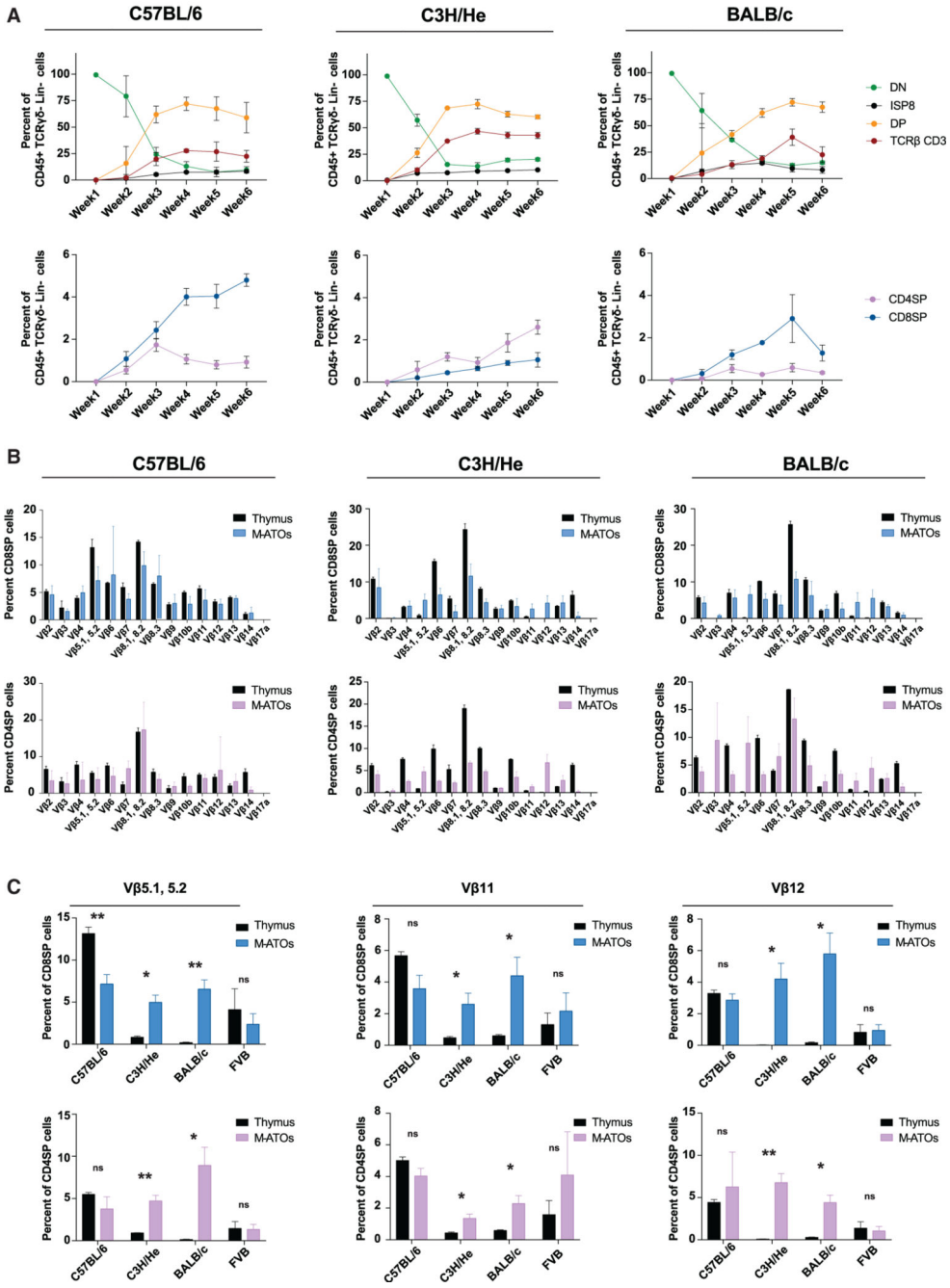

Figure 3. T Cell Differentiation and Maturation in M-ATOs from Different Murine Genetic Strains

(A) Frequencies of the different T cell populations generated in M-ATOs from LSK from the C57BL/6, C3H/He, and BALB/c backgrounds shown as percentage of total CD45$^+$ TCR$\gamma\delta^-$ Lin$^-$ cells over time. Error bars denote ±SD (C57BL/6, n = 6; C3H/He, n = 3; BALB/c, n = 3 independent experiments).

(B and C) TCR Vβ expression in T cells from thymus and M-ATOs from different murine genetic strains.

(B) TCR diversity in $CD3^+$ CD8SP (top) and $CD3^+$ CD4SP (bottom) T cells from week 6 M-ATOs or murine thymi, as shown by flow cytometry analysis of the frequency of TCR Vβ family expression in 3 murine backgrounds.

(C) Comparison of the Vβ5.1,5.2, Vβ11, and Vβ12 Vβ TCR segments expression in $CD3^+$ CD8SP (top) and $CD3^+$ CD4SP (bottom) T cells by flow cytometry in the thymus versus M-ATOs in four murine backgrounds.

Error bar denotes ± SD (C57BL/6 thymus, n = 4; C57BL/6 M-ATO, n = 5; C3H/He thymus, n = 4; C3H/He M-ATO, n = 4; BALB/c thymus, n = 4; BALB/c M-ATO, n = 5; FVB thymus, n = 4; FVB M-ATOs, n = 4 independent experiments). Significance: *$p < 0.05$, **$p < 0.01$, and ***$p < 0.001$ (multiple t tests).

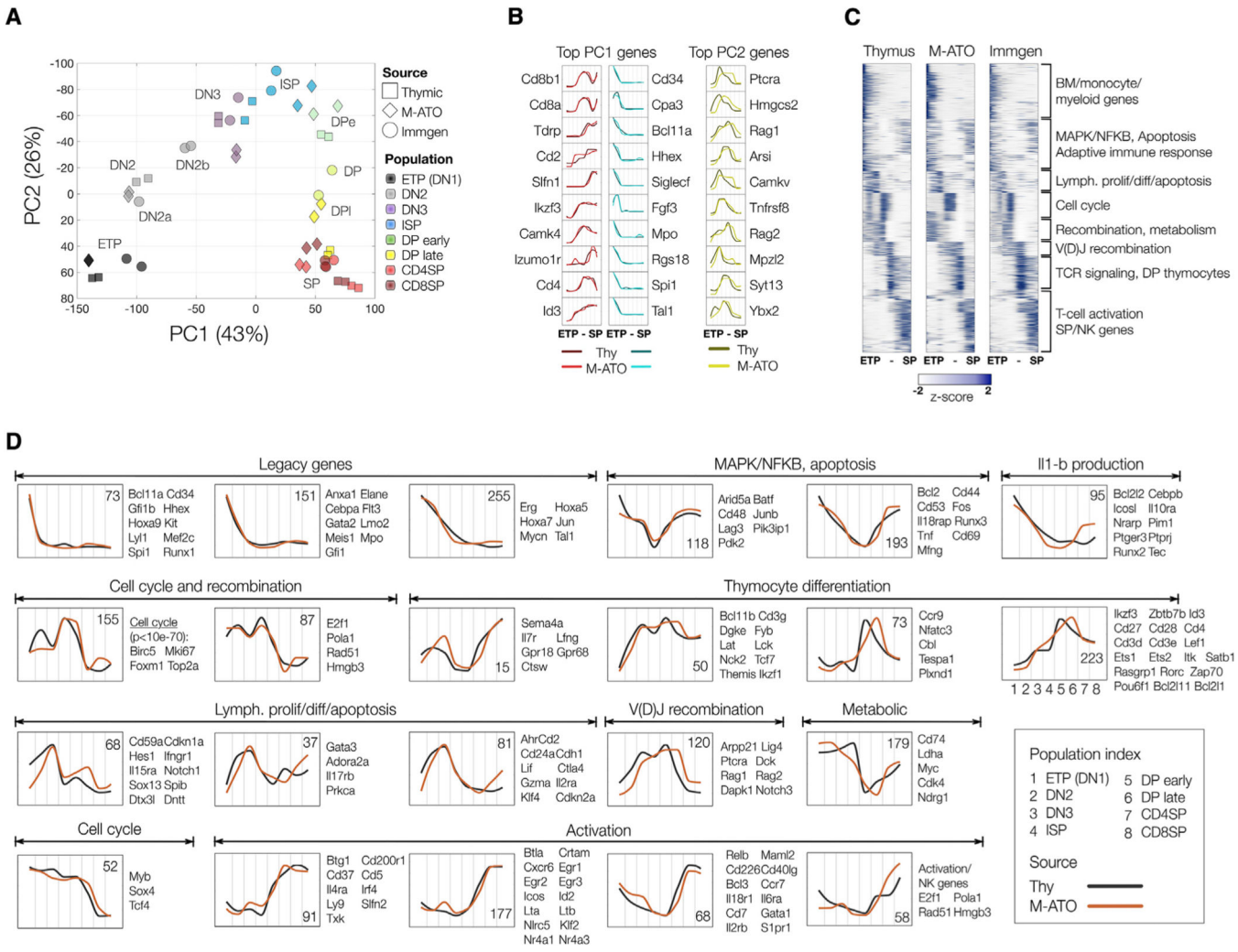

Figure 4. Transcriptional Regulation in M-ATO-Derived Thymocytes Recapitulates T Cell Developmental Programs *In Vivo*

(A) Principal-component analysis (PCA) of gene expression for M-ATO-derived and thymic populations. The first two components (PC1 and PC2) are shown along with the percentage of gene expression variance explained. Clustering was obtained with data from all detected genes without additional filters, using two independent replicates for samples generated in this work. Data from equivalent populations profiled by the Immgen consortium was mapped to the same PCA axes as an independent control. Phenotypes for all populations and sources shown are provided in Table S1. (Immgen data contained total DP rather than distinguishing early versus late.)

(B) Gene expression profile in M-ATO-derived and thymic populations for genes with high PCA loadings. For each gene and source, the y axis represents the average gene expression profile (two replicates per population) normalized to the mean expression across all populations. The x axis represents samples sorted as in (A), from progenitor (ETP) to mature single-positive (SP) T cells. Left: genes with the highest loadings on PC1. The top ten genes with increasing or decreasing gene expression are shown. Right: top ten genes with the highest loading on PC2.

(C) Hierarchical model-based clustering of 2,554 highly variable genes classified as differentially expressed (Wald-adjusted p value < 0.01, fold change > 4) within and between thymic and M-ATO-derived populations. The x axis represents samples sorted as in (A), and data for two biological replicates per sample are shown. Clustering was performed using raw count data, and each individual heatmap represents variance-stabilized gene expression data normalized as *Z*-scores. Annotations correspond to representative functional categories for genes in each major cluster.

(D) Hierarchical selected gene clusters and representative genes obtained from model-based analysis of highly variable genes. For each cluster, the average normalized profile in M-ATO-derived and thymic populations for all genes in the cluster is shown. The number of genes classified in each cluster is displayed in the inset. Clusters are grouped by overall gene expression trends and functional annotations. Representative genes in each cluster are highlighted; the full classification is provided in Table S1.

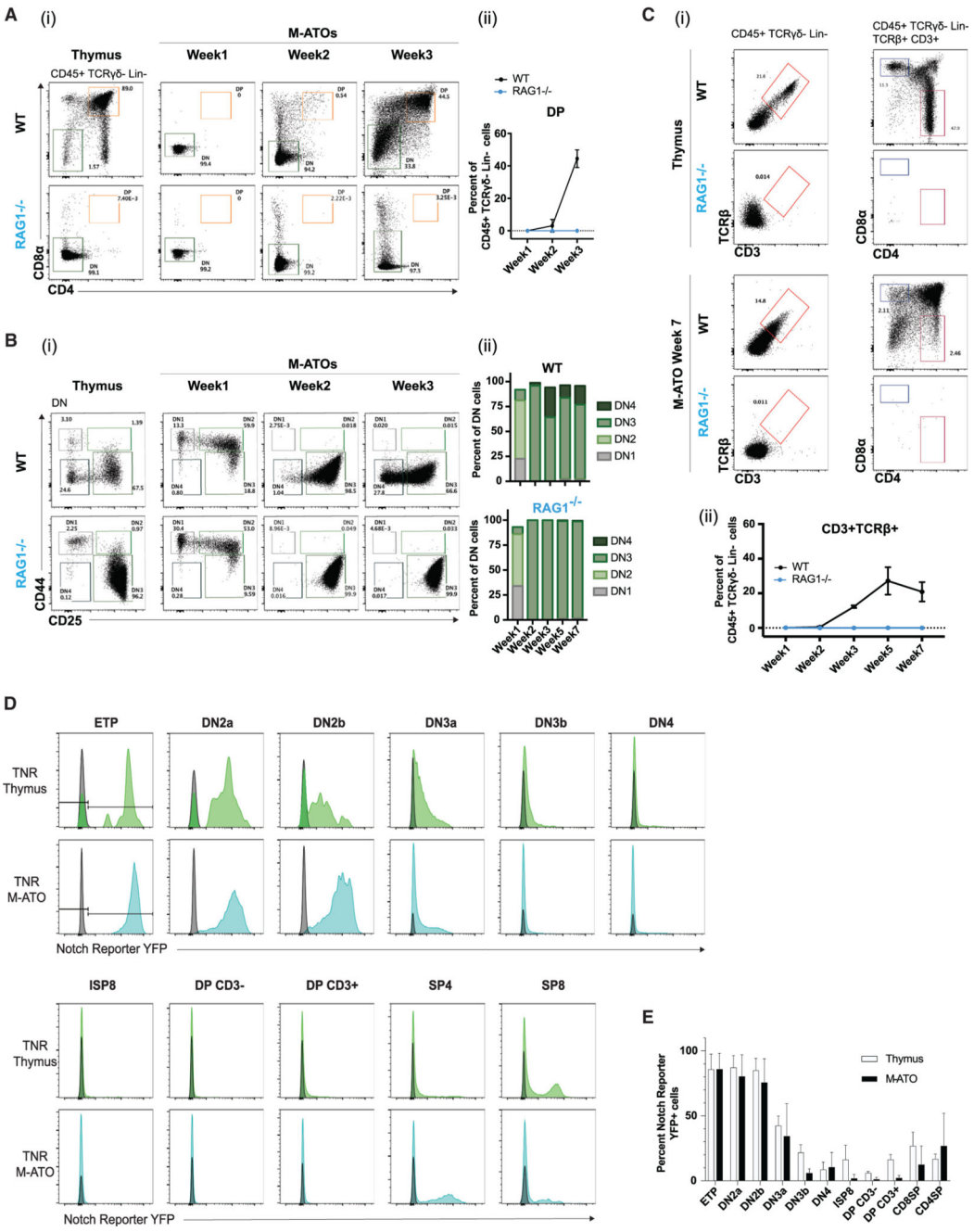

Figure 5. T Cell Differentiation in M-ATOs from Knockout and Reporter Murine Models Mimics the *In Vivo* Thymocyte Phenotype

(A–C) T cell differentiation in M-ATOs from LSK harvested from Rag1$^{-/-}$ and WT mice. Thymus phenotype is shown as comparison.

(A) (i) Representative kinetic analysis of DN and DP populations in M-ATOs. (ii) Frequency of DP population is shown as percentage of CD45^{+} TCR$\gamma\delta^{-}$ Lin^{-} cells.

(B) (i) Representative kinetic analysis of DN development in M-ATOs. (ii) Frequency of DN1–DN4 populations are shown as percentage of total DN cells.

(C) (i) TCR and CD3 expression in M-ATOs. (ii) Frequency of TCRβ^+CD3$^+$ population is shown as percentage of CD45$^+$ TCR$\gamma\delta^-$ Lin$^-$ cells. Significance: (i) Data are representative of three biological replicates. (ii) Error bars denote ± SD (n = 3 independent experiments).
(D and E) Notch activity in mouse thymus and M-ATO thymocyte populations using the transgenic Notch reporter (TNR) mouse model.
(D) Representative analysis of Notch reporter YFP expression levels in populations from the mouse thymus (top row, green) and M-ATO (bottom row, blue), shown in comparison with a negative control (gray).
(E) Frequency of TNR YFP$^+$ cells in each thymocyte population from mouse thymus (white bars) and M-ATO (black bars). Error bars denote ± SD (n = 6 independent experiments).

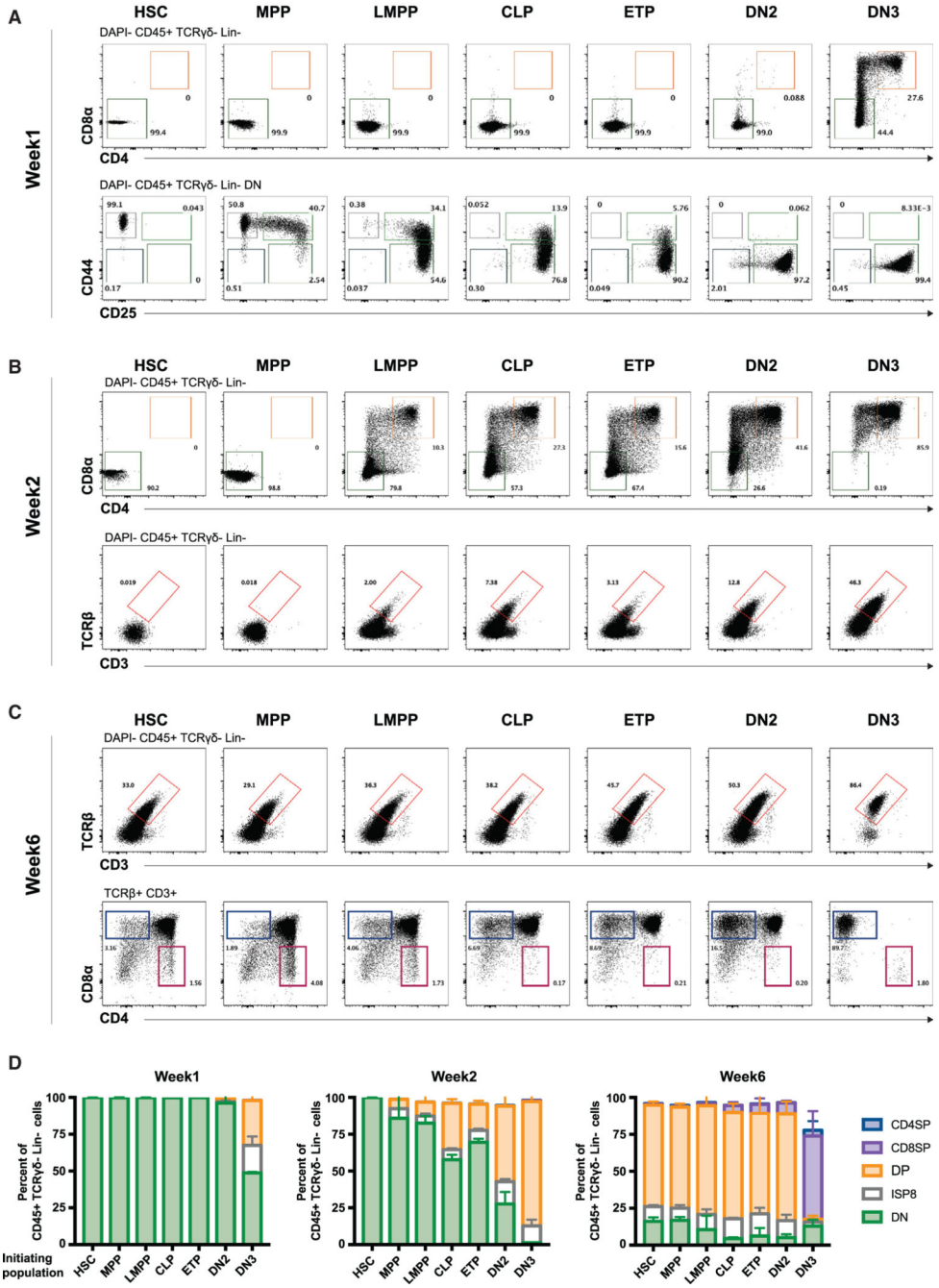

Figure 6. M-ATOs Recapitulate T Cell Differentiation from Different Hematopoietic Subsets

(A–C) Different subsets in the hematopoietic hierarchy from HSCs to T cell progenitors were isolated from the bone marrow and the thymus of C57BL/6 WT mice and seeded into M-ATOs. From the bone marrow: HSC (hematopoietic stem cell) ($Lin^{-}Sca1^{+}cKit^{+}CD48$ $CD150^{+}IL7R^{-}$); MPP (multi-potent progenitor) ($Lin^{-}Sca1^{+}c\text{-}Kit^{+}CD48^{-}CD150^{-}IL7R^{-}$); LMPP (lymphoid-primed multi-potent progenitor) ($Lin^{-}Sca1^{+}c\text{-}Kit^{+}IL7R^{+}Flk2^{+}$); and CLP (common lymphoid progenitor) ($Lin^{-}Sca1^{Lo}c\text{-}Kit^{Lo}$ $IL7R^{+}Flk2^{+}$). From the thymus: ETP ($Lin^{-}CD4^{-}CD8^{-}c\text{-}Kit^{hi}$ $CD44^{hi}CD25^{-}$); DN2 ($Lin^{-}CD4^{-}CD8^{-}c\text{-}Kit^{hi}$ $CD44^{hi}$ $CD25^{+}$); and

DN3 ($Lin^{-}CD4^{-}CD8^{-}CD44^{-}CD25^{+}$). Representative phenotypes of M-ATO-derived cells are shown at weeks 1 (A), 2 (B), and 6 (C). Data are representative of three biological replicates.

(D) Frequencies of T cell populations shown as percentage of total $CD45^{+}$ $TCR\gamma\delta^{-}$ Lin^{-} cells initiated from the different hematopoietic subsets in week 1, week 2, and week 6 M-ATOs. Error bars denote ± SD (n = 3 independent experiments).

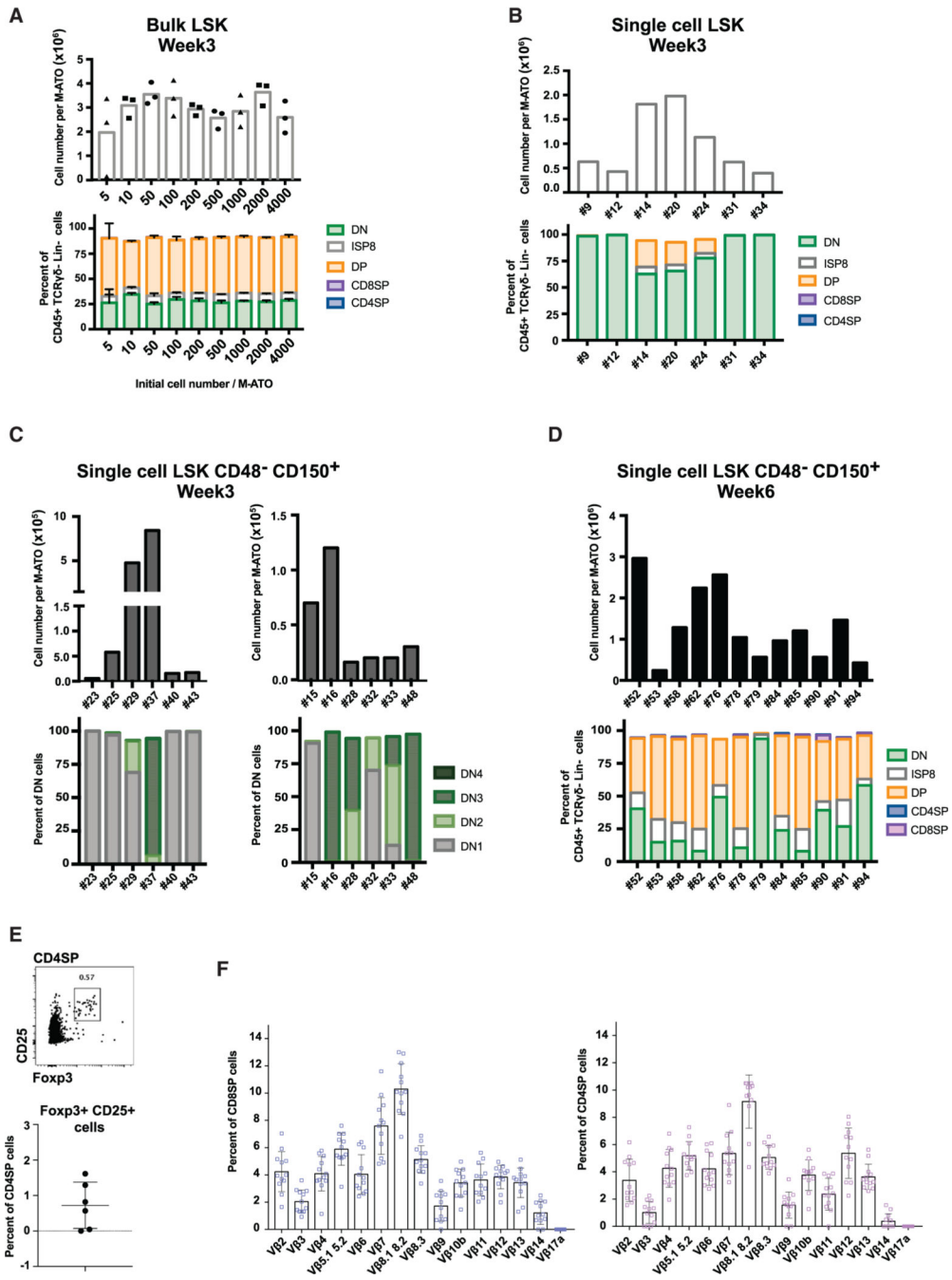

Figure 7. The M-ATO System Supports Full T Cell Differentiation from Isolated Single Cells

(A) Cell numbers and phenotype in week 3 M-ATOs initially seeded with different numbers of LSK isolated from C57BL/6 WT mice (5 to 4,000 cells per ATO). Top: total cell number per M-ATO. Bottom: frequency of cell populations as percentage of $CD45^+$ $TCR\gamma\delta^-$ Lin^- cells. Error bars denote ± SD (n = 3 independent experiments).

(B) Cell numbers (top) and phenotype (bottom) at week 3 in M-ATOs seeded with a single LSK cell from bone marrow. Seven independent M-ATOs are shown.

(C and D) Cell numbers (top) and phenotype (bottom) from weeks 3 (C) and 6 (D) M-ATOs initially seeded with a single (LSK $CD48^-$ $CD150^+$) HSC cell from C57BL/6 WT mice. Twelve independent M-ATOs are shown from two independent experiments (left and right).
(C) Frequencies of the DN1, DN2, DN3, and DN4 populations are shown as percentage of total DN cells, which represent 100% of the cells in week 3 M-ATOs.
(D) Frequencies of the T cell populations are shown as percentage of total $CD45^+$ $TCR\gamma\delta^-$ Lin^- cells in week 6 M-ATOs.
(E) Expression of the transcription factor Foxp3 via intracellular staining on CD4SP cells from thymocytes harvested from week 9 M-ATOs initially seeded with a single (LSK $CD48^-$ $CD150^+$) HSC. Frequencies of $Foxp3^+CD25^+$ Treg-like T cells are shown as percentage of total CD4SP T cells. $Foxp3^+CD25^+$ Treg-like T cells are detectable in five of six independent experiments.
(F) TCR diversity in $CD3^+$ CD8SP (left) and $CD3^+$ CD4SP (right) T cells from 12 week 6–7 M-ATOs generated from a single (LSK $CD48^-$ $CD150^+$) HSC as shown by flow cytometry analysis of the frequency of TCR Vβ family expression. Error bar denotes ± SD (n = 12 independent experiments).

KEY RESOURCES TABLE

REAGENT or RESOURCE	SOURCE	IDENTIFIER
Antibodies		
Anti-mouse CD3 (Clone145–2C11)	Biolegend	Cat# 100312, RRID:AB_312677
Anti-mouse CD4 (Clone RM4–5)	Biolegend	Cat# 100550, RRID:AB_2562099
		Cat# 100530, RRID:AB_389325
Anti-mouse CD5 (Clone 53–7.3)	Biolegend	Cat# 100627, RRID:AB_2563930
Anti-mouse CD8a (Clone 53–6.7)	Biolegend	Cat# 100708, RRID:AB_312747
		Cat# 100704, RRID:AB_312743
Anti-mouse CD11b (Clone M1/70)	Biolegend	Cat# 101228, RRID:AB_893232
Anti-mouse CD11c (Clone N418)	Biolegend	Cat# 117328, RRID:AB_2129641
Anti-mouse CD16/32 (TruStain FcX) (Clone 93)	Biolegend	Cat# 101320, RRID:AB_1574975
Anti-mouse CD19 (Clone 1D3/CD19)	Biolegend	Cat# 152406, RRID:AB_2629815
Anti-mouse CD25 (PC61)	Biolegend	Cat# 102016, RRID:AB_312865
Anti-mouse CD27 (LG.3A10)	Biolegend	Cat# 124226, RRID:AB_2565792
Anti-mouse CD28 (37.5)	Biolegend	Cat# 102127, RRID:AB_2650628
Anti-mouse CD44 (IM7)	Biolegend	Cat# 103059, RRID:AB_2571953
Anti-mouse CD45 (clone 30-F11)	Biolegend	Cat# 103116, RRID:AB_312981
Anti-mouse CD45R/B220 (Clone RA3–6B2)	Biolegend	Cat# 103236, RRID:AB_893354
Anti-mouse CD62L (MEL-14)	Biolegend	Cat# 104438, RRID:AB_2563058
Anti-mouse Ly-6G/Ly-6C (Gr-1) (Clone RB6–8C5)	Biolegend	Cat# 108428, RRID:AB_893558
Anti-mouse NK1.1 (Clone PK136)	Biolegend	Cat# 108728, RRID:AB_2132705
Anti-mouse interferon γ (Clone XMG1.2)	Biolegend	Cat# 505806, RRID:AB_315400
Anti-mouse IL-2 (Clone JES6–5H4)	Biolegend	Cat# 503826, RRID:AB_2650897
Anti-mouse TCRβ (Clone H57–597)	Biolegend	Cat# 109234, RRID:AB_2562350
		Cat# 109208, RRID:AB_313431
Anti-mouse TCRγδ (Clone GL3)	Biolegend	Cat# 118120, RRID:AB_2562566
Anti-mouse TNFα (Clone MP6-XT22)	Biolegend	Cat# 506339, RRID:AB_2563127
Anti-mouse TER-119 (clone Ter119)	Biolegend	Cat# 116228, RRID:AB_893636
Anti-mouse CD150 (Clone TC15–12F12.2)	Biolegend	Cat# 115941, RRID:AB_2629660
Anti-mouse CD117 (c-KIT) (Clone ACK2)	Biolegend	Cat# 135122, RRID:AB_2562042
Anti-mouse Ly-6A/E (Sca-1) (Clone D7)	Biolegend	Cat# 108114, RRID:AB_493596
Anti-mouse CD48 (Clone HM48–1)	Biolegend	Cat# 103432, RRID:AB_2561463
Anti-mouse CD127 (IL-7R) (Clone REA680)	Miltenyi Biotech	Cat# 130–122-938, RRID:AB_2783928
Anti-mouse CD135 (Flk-2) (Clone A2F10)	Biolegend	Cat# 135306, RRID:AB_1877217
Anti-mDLL4 (clone HMD4–1)	Biolegend	Cat# 130813, RRID:AB_2246026
Anti-GFP (clone FM264G)	Biolegend	Cat# 338001, RRID:AB_1279415
AlexaFluor-594-conjugated donkey anti-rat IgG (H+L)	Jackson ImmunoResearch	Cat# 712–585-150, RRID: AB_2340688
AlexaFluor-488-conjugated donkey anti-rat IgG (H+L)	Jackson ImmunoResearch	Cat# 712–545-150, RRID: AB_2340683
Biotin-SP (long spacer) AffiniPure Goat Anti-Armenian Hamster IgG (H+L)	Jackson ImmunoResearch	Cat# 127–065-160, RRID: AB_2338980
AlexaFluor-594-conjugated Streptavidin	Jackson ImmunoResearch	Cat# 016–580-084, RRID: AB_2337250

REAGENT or RESOURCE	SOURCE	IDENTIFIER
Bacterial and Virus Strains		
pCCL-c-MNDU3-mDLL4 (lentivirus)	This paper	N/A
pCCL-c-MNDU3-mDLL4-IRES-eGFP (lentivirus)	This paper	N/A
Chemicals, Peptides, and Recombinant Proteins		
rmIL-2	Peprotech	Cat# 212–12
rmIL7	Peprotech	Cat# 217–17
rmSCF	Peprotech	Cat# 250–03
rmFlt3L	Peprotech	Cat# 250–31L
Beta Mercapto Ethanol (bME)	Sigma-Aldrich	Cat# M7522
L-Ascorbic Acid 2-phosphate sequimagnesium salt hydrate	Sigma-Aldrich	Cat# A8960–5G
B27 supplement	ThermoFisher Scientific	Cat# 17504–044
DAPI	Life technologies	Cat# D1306
Formaldehyde	Sigma-Aldrich	Cat# F8775
Vectashield Antifade Mounting Medium	Vector Laboratories	Cat# H1000
Critical Commercial Assays		
Direct mouse Lin depletion Kit	Miltenyi Biotech	Cat# 130–110-470
CD8 selection kit	Miltenyi Biotech	Cat# 130–104-075
CD4 isolation kit	Miltenyi Biotech	Cat# 130–104-454
CD62L isolation kit	Miltenyi Biotech	Cat# 130–091-758
Anti-mouse TCR Vβ screening panel	BD Bioscience	Cat# 557004
Cell Stimulation Cocktail (plus protein transport inhibitors)	eBioscience	*Cat# 00–4975-03*
Intracellular Fixation & Permeabilization Buffer Set	eBioscience	*Cat# 88–8824-00*
True-Nuclear Transcription Factor Buffer Set	Biolegend	*Cat# 424401*
Cell Trace Violet cell proliferation assay	Invitrogen	Cat# C34557
Dynabeads Mouse T cell activation CD3/CD28	GIBCO ThermoFisher	Cat# 11456D
RNeasy Micro kit	QIAGEN	Cat# 74004
SMARTer Stranded Total RNA-Seq (Pico) Kit	Clonetech	Cat# 635005
Deposited Data		
Raw and analyzed data	This paper	GSE146224
Experimental Models: Cell Lines		
MS5-mDLL4	This paper	N/A
MS5-mDLL4-eGFP	This paper	N/A
Experimental Models: Organisms		
Mouse: C57BL/6J	The Jackson Laboratory	Cat# JAX:000664, RRID:IMSR_JAX:000664
Mouse: B6.Cg-*Foxp3*$^{tm2(EGFP)Tch}$/J, B6-Foxp3^{EGFP}	The Jackson Laboratory	Cat# JAX:006772, RRID:IMSR_JAX:006772
Mouse: B6.129S7-*Rag1*^{tm1Mom}/J	The Jackson Laboratory	Cat# JAX:002216, RRID:IMSR_JAX:002216
Mouse: BALB/cJ	The Jackson Laboratory	Cat# JAX:000651, RRID:IMSR_JAX:000651

REAGENT or RESOURCE	SOURCE	IDENTIFIER
Mouse: C3H/HeJ	The Jackson Laboratory	Cat# JAX:000659, RRID:IMSR_JAX:000659
Mouse: FVB/NJ	The Jackson Laboratory	Cat# JAX:001800, RRID:IMSR_JAX:001800
Mouse: Tg(Cp-HIST1H2BB/Venus)47Hadj/J	The Jackson Laboratory	Cat# JAX:020942, RRID:IMSR_JAX:020942
Software and Algorithms		
FlowJo	Tree Star Inc.	https://www.flowjo.com/solutions/flowjo
GraphPad Prism	GraphPad Software	https://www.graphpad.com/scientific-software/prism/
bcl2fastq2 (v2.17)	Illumina	https://support.illumina.com/downloads/bcl2fastq-conversion-software-v2–20.html
The *STAR* ultrafast universal RNA-seq aligner v2.5.2b	Dobin et al., 2013	N/A
DESeq2	Love et al., 2014	https://bioconductor.org/packages/release/bioc/html/DESeq2.html
Metascape	Metascape	http://metascape.org
Cytoscape	Shannon et al., 2003	https://www.cytoscape.org/
MATLAB	The MathWorks, Inc	https://www.mathworks.com/products/matlab.html
R	R	https://www.R-project.org/
Zen	Zeiss	https://www.zeiss.com/microscopy/int/products/microscope-software/zen.html
Fiji	NIH image	https://imagej.net/Fiji